Chapter 8
Measurement-Based Methods for Model Reduction of Power Systems Using Synchrophasors

Aranya Chakrabortty and J. Chow

Abstract Wide-area analysis and control of large-scale electric power systems are highly dependent on the idea of *aggregation*. For example, one often hears power system operators mentioning how "Northern Washington" oscillates against "Southern California" in response to various disturbance events. The main question here is whether we can analytically construct dynamic electromechanical models for these conceptual, aggregated generators representing Washington and California, which in reality are some hypothetical combinations of hundreds of actual generators. In this chapter we present an overview of several new results on how to construct such simplified interarea models of large power systems by using dynamic measurements available from phasor measurement units (PMUs) installed at limited points on the transmission lines. Our examples of study are motivated by widely encountered power transfer paths in the Western Electricity Coordinating Council (WECC), namely a two-area radial system representing the WA-MT flow, a star-connected three-area system resembling the Pacific AC Intertie, and a generic multi-area system with more than one dominant slow mode of oscillation.

8.1 Introduction

Over the past few years, several catastrophic phenomena, such as cascade failures and blackouts in different parts of the North American power grid, have forced power system researchers to look beyond the traditional approach of analyzing power system functionalities in *steady-state*, and instead pay serious attention to their

A. Chakrabortty (✉)
North Carolina State University, Raleigh, NC, USA
e-mail: aranya.chakrabortty@ncsu.edu

J. Chow
Rensselaer Polytechnic Institute, Troy, NY, USA
e-mail: chowj@rpi.edu

J. H. Chow (ed.), *Power System Coherency and Model Reduction*,
Power Electronics and Power Systems 94, DOI: 10.1007/978-1-4614-1803-0_8,

dynamic characteristics, and in a global or *wide-area* sense. This mindset has been particularly facilitated by the recent outburst of measurement and instrumentation facilities in the context of smart power grids provided by the wide-area measurement system (WAMS) technology, which uses sophisticated digital recording devices called phasor measurement units (PMUs) to record and export GPS-synchronized high-sampling-rate (6–60 samples/s) dynamic power system data [1]. Industry platforms, such as the North American Synchrophasor Initiative (NASPI) [2], have been formed to investigate ways by which PMU measurements from different parts of the US power system can possibly be exploited to gain insight into their dynamic interdependence, which could indicate how events in one area of the grid can propagate and have a significant impact on other remote areas.

However, a major road-block to wide-area analysis of large-scale power systems is the absence of concrete mathematical models that capture the aggregated electromechanical dynamics coupling one area of the system with another. For example, one often hears power system operators mentioning how "Northern Washington" oscillates against "Southern California" in response to various disturbance events. The main question here is whether we can analytically construct dynamic electromechanical models for these conceptual, aggregated generators representing Washington and California, which in reality are some hypothetical combinations of hundreds of actual generators. For example, it is well known that a 0.25 Hz interarea swing mode exists between the north–south interconnections of the Western Electricity Coordinating Council (WECC) extending from Alberta, Canada to Baja Mexico [3], with additional 0.4–0.7 Hz modes along the pacific AC intertie and the east–west interconnection. Based on such interarea modal behavior, conceptually speaking, the map of WECC can be drawn as an equivalent mass-spring-damper model [4], as in Fig. 8.1a, showing how the electromechanical dynamics of the aggregated parts of WECC may swing against each other when a disturbance sets in. Figures 8.1b and c shows the partitioning of the WECC into a 2-area system and a 9-area system. But, again, the main question to be resolved is how can we construct an explicit dynamic model for this conceptual figure, preferably in real-time, using voltage, current, or power flow signal measurements in order to establish a prototype for the nonlinear interarea dynamics of the entire interconnection. Using conventional model-based equivalencing methods [5] would be impractical for this purpose because they are highly time-consuming and numerically challenging for large-scale nonlinear simulations. More importantly, they are dependent on the precise knowledge of the model parameters (such as inertia, transient reactance, transformer reactance) of all the thousands of generators, transmission lines, and loads constituting each aggregate area.

Motivated by these fundamental questions of current interest to the PMU research community, in this chapter we develop a framework for the identification of reduced-order dynamic models of very large-scale power systems, not by using traditional model-based methods [5], but from synchrophasor measurements available from PMUs installed only at selected points on the transfer path. Our models of study in this chapter represent prototypes of three well-known transfer paths in the WECC, namely,

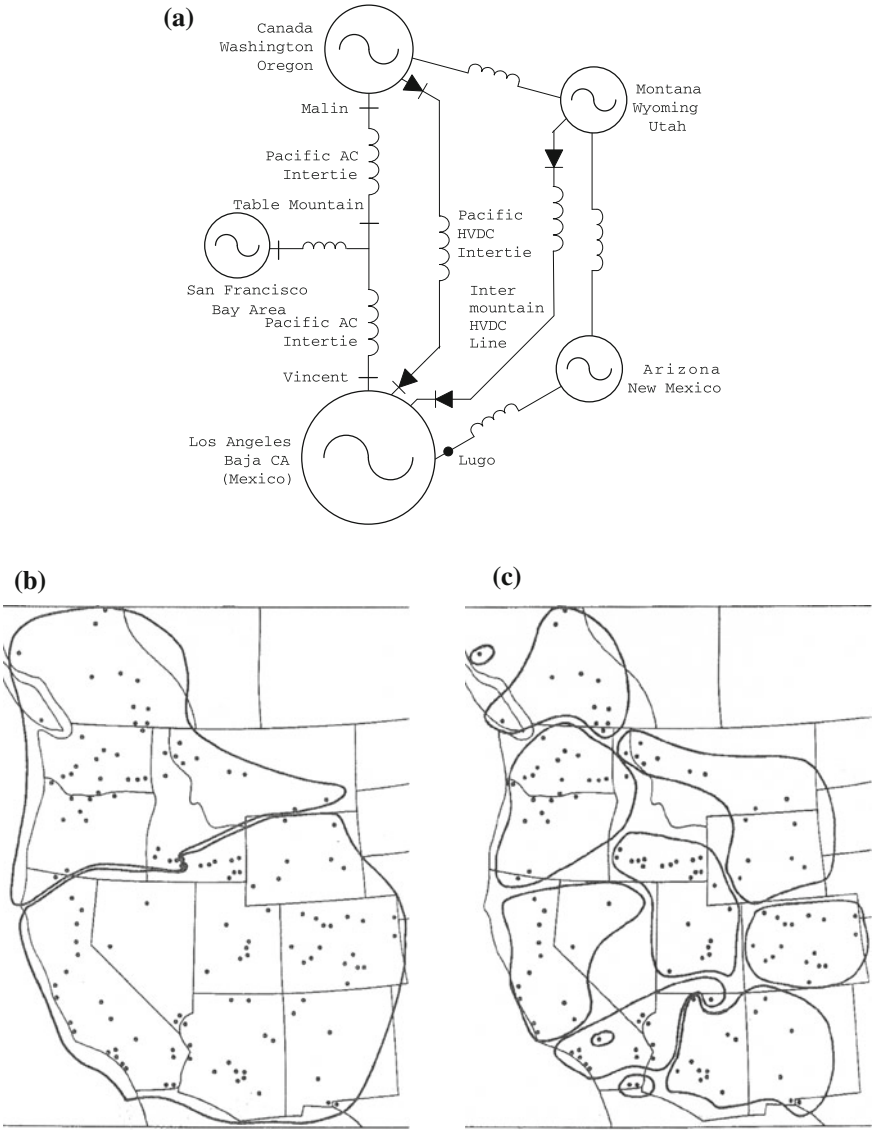

Fig. 8.1 Area aggregations in Western Electricity Coordinating Council (*WECC*). **a** Spring-mass system representation of WECC. **b** WECC 2-area partition. **c** WECC 9-area partition

1. One-dimensional models such as a two-area radial system with one dominant slow mode of oscillation (e.g., Washington-Montana transfer),
2. Two-dimensional models with algebraic nodes such as a three-area star-connected system with one or two dominant slow modes of oscillation (e.g., Pacific AC intertie),

3. Two-dimensional models with direct connectivity, i.e., a general multi-area power system with a given *interarea* topology, and two or more slow modes of oscillation.

For each of these transfer paths, we first show that the model identification reduces to a parameter estimation problem for the aggregated *intra-area* reactances and machine inertias internal to each area, and then derive analytical results showing how the voltage, phase angle, and frequency oscillations at multiple buses on the transfer path, following a small-signal disturbance, can be used to estimate these parameters. We illustrate our results with real power system disturbance events in WECC. The objective of this chapter should not, however, be confused with research on *modal identification*, the purpose of which is to estimate the eigenvalues and eigenvectors of the state matrix of the linearized power system from the measured states. Several numerical algorithms have been developed for such mode estimation from both *ringed-down* disturbance data and ambient measurements, as discussed in the seminal work of Hauer [6, 7] with established applications in wide-area monitoring in the US as well as in other countries, such as Australia [8, 9], China [10], and Denmark [11]. This chapter, on the other hand, looks farther beyond mode estimation towards identifying dynamic model parameters from the "modes".

The remainder of the chapter is organized as follows. Sections 8.2, 8.3, and 8.4 pose the interarea model estimation (IME) problem for one- and two-dimensional systems together with the validations of the respective results through PMU data analysis of WECC. Section 8.5 presents transient stability assessment using these equivalent models via energy function analysis, while Sect. 8.6 develops PMU placement methods using noisy data. Section 8.7 concludes the chapter.

8.2 Problem Formulation

Mathematical modeling of dynamic equivalents of large-scale electric power systems has seen some 40 years of long and rich research history. The foundations of this line of research were laid in the late 1970s by Chow and Kokotović, who introduced the ideas of *aggregation* and *coherency* [5], resulting in algorithms of partitioning a power network into dynamic aggregates, where each aggregate consists of a group of strongly connected generators that synchronize over a fast time-scale and, thereafter, act as a single entity, while the aggregates themselves are weakly connected to each other, and synchronize over a slower time-scale. Using singular perturbation theory, they derived analytical expressions for aggregated machine inertias and reactances in terms of the model parameters of each individual machine contained in an area. Their approach was complemented by alternative techniques of coherency such as those by Germond and Podmore [12], and de Mello, Podmore, and Stanton using circuit-theoretic approaches [13], Undrill and Turner using linear modal decomposition [14], Zaborszky et al. using enumerative clustering algorithms [15], and Nath et al. using iterative techniques to compute the coupling strengths between different areas [16]. Aggregation and coherency reduced the computational complexities of solving thousands of nonlinear equations in power system stability programs from detailed

models, and was tested offline on both small-scale (such as the 48-machine NPCC system[1]) and large-scale (such as the 12,000-bus NYPP system[2]) via software programs such as *DYNEQ* and *DYNRED* [17]. However, the main limitations of the above-mentioned conventional model reduction methods are twofold: first, they are *model-based* methods, meaning that to construct reduced-order models using these methods one would need to know each constituent model explicitly; and second, in constructing an aggregate motion, most of these methods tend to capture minute details of the fast local oscillations in each area that not only increase the computational time but also may be unnecessary at times of emergency when decisions have to be made fast.

The methods proposed in this chapter are meant to circumvent these traditional barriers by developing model reduction algorithms that do not depend on individual component-level model information, and are based on measurements only. PMU measurements of voltage, current and frequency from disturbance events available from a limited number of points in the network will be utilized for this purpose. Our first system of investigation is a commonly encountered power transfer path, namely, a two-area radial power system, as shown in Fig. 8.2a, containing multiple strongly connected machines in each area with arbitrary interconnection structure. Its two-machine dynamic (interarea) model and its classical circuit representation are shown in Fig. 8.2b. The system consists of two aggregated generators G_1 and G_2, which represent coherent combinations of strongly connected machines in each respective area. Let the equivalent inertias of these aggregated machines be H_1 and H_2, respectively. The machines are connected to the high-voltage terminal buses 1 and 2 through equivalent transformers having reactances x_{T1} and x_{T2}, which, in turn, represent Thevenin equivalents of the transformer reactances in each respective area. This two-area system is useful for representing a radial transfer path in a large power system in which one coherent area is exporting power to the other coherent area. The voltage phasors at Buses 1 and 2 are given as

$$\tilde{V}_i = V_i \angle \theta_i, \quad i = 1, 2 \tag{8.1}$$

where $V\angle\theta$ denotes the polar representation $V\varepsilon^{j\theta}$. The transmission line between Buses 1 and 2 is assumed to be lossless with a reactance x_e. The line current flowing from Bus 1 to Bus 2 is $\tilde{I} = I\angle\theta_I$ with G_1 supplying power to G_2, which acts as a load. For the classical model representation, the internal voltages of the generators G_1 and G_2 are denoted as

$$\tilde{E}_1 = E_1 \angle \delta_1, \quad \tilde{E}_2 = E_2 \angle \delta_2. \tag{8.2}$$

The total reactances connecting the generator internal voltage nodes to the terminal Buses 1 and 2 are given as

[1] Northeast Power Coordinating Council.

[2] New York Power Pool.

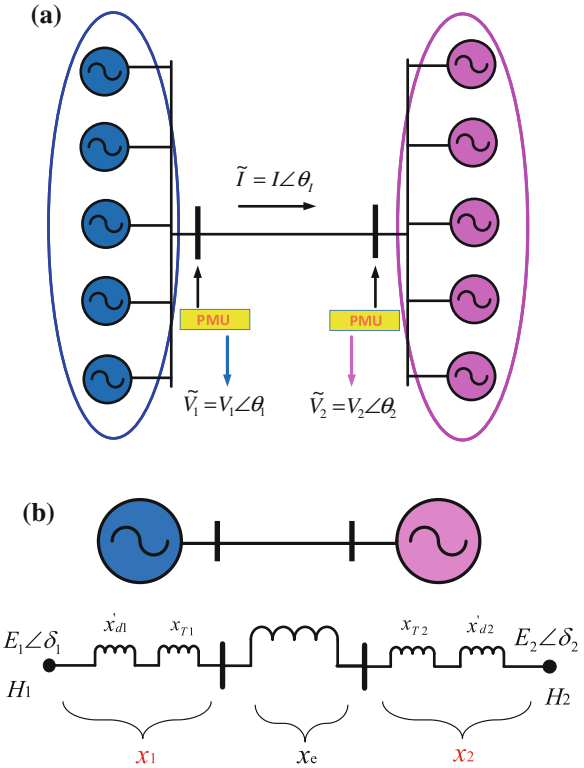

Fig. 8.2 Area aggregations in Western Electricity Coordinating Council (*WECC*). **a** Two-area power system. **b** Two-machine interarea equivalent

$$x_i = x_{Ti} + x'_{di}, \quad i = 1, 2 \tag{8.3}$$

where x'_{d1} and x'_{d2} are the equivalent direct-axis transient reactances of G_1 and G_2, respectively. The total reactance of the transfer path is, therefore, given as

$$\bar{x} = x_1 + x_e + x_2. \tag{8.4}$$

The electromechanical model of each aggregated generator, neglecting damping, can be written as [18]

$$\dot{\delta}_i = \Omega(\omega_i - \omega_s), \quad 2H_i\dot{\omega}_i = P_{mi} - P_{ei}, \quad i = 1, 2, \tag{8.5}$$

where $\Omega = 120\pi$ for a 60 Hz system, ω_s is the synchronous speed, and ω_i, P_{mi}, P_{ei} are, respectively, the angular velocity, the mechanical power input, and the electrical power output of the i^{th} machine. All quantities are in per unit except for the phase angles which are in radians. We assume that inside each area the system configuration

remains unchanged over the time-scale of the interarea mode. The two swing equations in (8.5) can then be combined to form a second-order system

$$\dot{\delta} = \Omega\,\omega, \quad 2H\,\dot{\omega} = P_m - P_e \tag{8.6}$$

with

$$P_m = \frac{H_2 P_{m1} - H_1 P_{m2}}{H_1 + H_2}, \quad P_e = \frac{E_1 E_2}{\bar{x}} \sin(\delta) \tag{8.7}$$

where $H = H_1 H_2/(H_1 + H_2)$ is the equivalent inertia, $\delta = \delta_1 - \delta_2$, and $\omega = \omega_1 - \omega_2$. Assuming that PMU measurements of voltage, current, and bus frequency are available from Buses 1 and 2, we then pose the problem of finding the reduced model in Fig. 8.2b as follows.

Given the measured synchronized phasor variables V_1, θ_1, V_2, θ_2, I, *and* θ_I *in* Fig. 8.2a *that exhibit a few cycles of interarea oscillations, compute* E_i, δ_i, x_i, *and* H_i, $i = 1, 2$, *and* x_e *of the reduced-order two-machine system in* Fig. 8.2b *to represent the interarea dynamic behavior of the two-area power system.*

Because $\tilde{V}_1$, $\tilde{V}_2$ and $\tilde{I}$ are measured, x_e can be easily computed from $jx_e = (\tilde{V}_1 - \tilde{V}_2)/\tilde{I}$. Similarly $\tilde{E}_1$ and $\tilde{E}_2$ can be computed if x_1 and x_2 are known. Therefore, the above problem, referred to as the Interarea Model Estimation (IME) problem, reduces to the estimation of four quantities, namely x_1, x_2, H_1, and H_2. We next derive algorithms by which these four parameters can be identified from the interarea oscillations of voltage and frequency captured by the PMUs on the transfer path.

8.2.1 Reactance Estimation

Without any loss of generality, we fix our reference at the internal node of Generator 2, and assume $\delta_2 = 0$ and $\delta_1 = \delta$. The first step for this algorithm is to choose any phasor variable measured by the PMUs, for example, magnitude of bus voltages. The voltage phasor at any point P at a reactance jx away from Generator 2 (or equivalently at a distance x away if the reactance is uniformly distributed along the path), can be written as

$$\tilde{V} = a\,E_1(\cos(\delta) + j\,\sin(\delta)) + E_2(1 - a) \tag{8.8}$$

where $a = x/(x_1 + x_e + x_2)$ is the normalized reactance of the point P. The magnitude of $\tilde{V}(x)$, denoted as V, is, therefore,

$$V \triangleq |\tilde{V}| = \sqrt{c + 2E_1E_2((a - a^2)\cos(\delta))} \tag{8.9}$$

where $c = (1-a)^2E_2^2 + a^2E_1^2$. Considering a small-signal disturbance in the system, and linearizing (8.6) and (8.9) about an equilibrium point (δ_0, $\omega_0 = 0$, V_{ss}), any

change in V can be written as

$$\Delta V(a,t) = \frac{-E_1 E_2 \sin(\delta_0)(a-a^2)}{V(a,\delta_0)} \Delta\delta(t). \tag{8.10}$$

Of prime importance is that the Jacobian in (8.10) consists of two parts: a numerator part varying with a, and a denominator part which is the steady-state bus magnitude at the point P. From (8.10), we can write

$$V_n \triangleq \Delta V(a,t) V(a,\delta_0) = A\, a(1-a)\Delta\delta(t). \tag{8.11}$$

where $A = -E_1 E_2 \sin(\delta_0)$. The quantity V_n in (8.11), referred to as the *normalized voltage* is a product of two quantities, namely the change in voltage at the point P at any time instant t following the disturbance from the predisturbance equilibrium voltage $V(a,\delta_0)$ at this point, and $V(a,\delta_0)$ itself. If a PMU is located at this point P, then both of these quantities and, therefore, the normalized voltage can be calculated from the PMU measurement recordings at any fixed point of time. The RHS of (8.11) consists of the unknown constant A as well as the hypothetical state evolution $\Delta\delta(t)$, which depends only on time t and not on the spatial variable a. We refer to this as the *time–space separation* property, using which we can simply write

$$\frac{V_{n1}(a_1,t^*)}{V_{n2}(a_2,t^*)} = \frac{a_1(1-a_1)}{a_2(1-a_2)} \tag{8.12}$$

where V_{n1} and V_{n2} are, respectively, the normalized voltages at Bus 1 and Bus 2, t^* is a fixed point of time, while

$$a_1 = \frac{(x_2+x_e)}{(x_1+x_e+x_2)}, \quad a_2 = \frac{x_2}{(x_1+x_e+x_2)} \tag{8.13}$$

are the normalized reactances of these two respective buses. To generate a second equation we need another measurement point, which, in other words, indicates that we must have a third PMU installed at some intermediate bus on the transfer path between Bus 1 and Bus 2 at a known distance from Bus 2. In that case, for the same time instant $t = t^*$ as before, we can use

$$\frac{V_{n3}(a_3,t^*)}{V_{n2}(a_2,t^*)} = \frac{a_3(1-a_3)}{a_2(1-a_2)} \tag{8.14}$$

where a_3 is the normalized reactance corresponding to the third bus. Equations (8.12) and (8.14) can then be solved for x_1 and x_2 using numerical algorithms. If damping is considered in (8.6), then additionally we will have to consider one more data point and form a third equation similar to (8.14).

Note 1: Even if an actual PMU is not installed between buses 1 and 2, a third voltage $\tilde{V}_3$ can still be obtained using the relation $\tilde{V}_3 = \tilde{V}_2 + jx_{23}\tilde{I}$, where x_{23} is the

reactance between the third point and Bus 2 (and is assumed to be known), while $\tilde{I}$ is the line current measured by the PMU at Bus 2.

Note 2: If the transmission line has both resistance and reactance, then the spatial variable a simply needs to be defined as a ratio of the impedance of any point measured from Bus 2 to the total impedance of the transfer path. The rest of the algorithm will not change under that situation.

8.2.2 Inertia Extrapolation Algorithm

Once x_1 and x_2 have been computed, the remaining parameters to be computed are the inertias H_1 and H_2. We need two pieces of information. First, by measuring the frequency f of the swing mode in the voltage measurement (which can be done using modal decomposition algorithms), the equivalent inertia constant H can be computed from linear circuit theory as [18]

$$H = (E_1 E_2 \cos(\delta_0)\Omega)/(2\,\bar{x}\,(2\pi f)^2) \tag{8.15}$$

Second, to calculate H_1 and H_2 separately, we develop a companion equation by exploiting the frequencies measured at Buses 1 and 2. Neglecting losses and machine damping effects, the conservation of the total angular momentum of the two-machine system is given as

$$\begin{aligned} L &= 2H_1\omega_1 + 2H_2\omega_2 = 2\int (H_1\dot{\omega}_1 + H_2\dot{\omega}_2)\,\mathrm{d}t \\ &= \int (P_{m1} - P_{e1} + P_{m2} - P_{e2})\,\mathrm{d}t = 0 \end{aligned} \tag{8.16}$$

from which we obtain

$$\frac{H_1}{H_2} = -\frac{\omega_2}{\omega_1} \tag{8.17}$$

Hence, (8.17) can be used to solve for H_1 and H_2, provided that the estimates for the machine speeds are known. For the two-machine system, we can show that ω_1 and ω_2 can indeed be estimated from the measured frequencies ϑ_1 and ϑ_2 at Buses 1 and 2 according to the equations

$$\vartheta_1 = \frac{g_1\omega_1 + h_1(\omega_1 + \omega_2)\cos(\delta_1 - \delta_2) + k_1\omega_2}{g_1 + 2h_1\cos(\delta_1 - \delta_2) + k_1} \tag{8.18}$$

$$\vartheta_2 = \frac{g_2\omega_1 + h_2(\omega_1 + \omega_2)\cos(\delta_1 - \delta_2) + k_2\omega_2}{g_2 + 2h_2\cos(\delta_1 - \delta_2) + k_2} \tag{8.19}$$

where $g_1 = E_1^2(1-\rho_1)^2$, $h_1 = E_1E_2\rho_1(1-\rho_1)$, $k_1 = \rho_1^2E_2^2$, $g_2 = E_1^2(1-\rho_2)^2$, $h_2 = E_1E_2\rho_2(1-\rho_2)$, and $k_2 = \rho_2^2E_2^2$, with $\rho_1 = x_1/\bar{x}$ and $\rho_2 = (x_1+x_e)/\bar{x}$. Equations (8.18–8.19) can be derived simply from (8.8) by considering $\theta = \tan^{-1}(\mathrm{Im}(\tilde{V})/\mathrm{Re}(\tilde{V}))$, and then taking the time derivative to derive $\vartheta = \dot{\theta}$ as a function of a. Because the bus frequencies ϑ_1 and ϑ_2 are available from PMU measurements, we can estimate ω_1 and ω_2 using (8.18) and (8.19), calculate the ratio $\omega_2/\omega_1 = -H_1/H_2$, and solve for H_1 and H_2 using (8.15) and the relation $H = H_1H_2/(H_1+H_2)$.

8.2.3 Washington-Montana Transfer Path Modeling

We next model the east–west WECC power transfer between the aggregated generators of "Canada, Washington, Oregon" and "Montana, Wyoming, Utah" indicated in Fig. 8.1a, referred to here as *WECC transfer path* 1. The system consists of a median-size group of remote machines supplying power via a 600-mile transmission system to a load center. A disturbance initiated a 0.578 Hz oscillation across the transfer path. The event recording started 60 s before the disturbance for a total of 5 min. We assume that the transmission line is lossless. The variation of the voltage magnitudes at the two terminal buses and the midpoint over time are shown by the field measured data in Fig. 8.3a. We separate the fast and slow components of the voltage waves by bandpass filtering, as shown in Fig. 8.3b and c. The upper and lower cut-offs of the filter are chosen as 1 and 0.2 Hz, respectively, covering the interarea mode frequency. In Fig. 8.3b, we show the voltage oscillations from time $t = 60$–90 s. In this figure we can see that the oscillations are not exactly sinusoidal due to the presence of local modes in addition to the interarea mode. To extract the interarea mode, we apply the eigenvalue realization algorithm (ERA) on the three bus voltages [19]. Figures 8.4a and b shows the comparison of the interarea oscillations with the measured bus voltages at Buses 1 and 2. The oscillations are now free from the distortions due to the local mode effects, and are purely sinusoidal. Choosing a fixed time instant of $t = 75$ s, the amplitudes of the interarea oscillations at the respective buses are then measured as

$$V_{1m} = 8.746 \times 10^{-3},\ V_{2m} = 9.733 \times 10^{-3},\ V_{3m} = 0.01845 \tag{8.20}$$

The pre-disturbance equilibrium voltages are measured as

$$V_{1\mathrm{ss}} = 1.082,\ V_{2\mathrm{ss}} = 1.087,\ V_{3\mathrm{ss}} = 1.089 \tag{8.21}$$

Therefore, the normalized amplitude of oscillations are

$$V_{1n} = 9.46 \times 10^{-3},\quad V_{2n} = 1.06 \times 10^{-3},\quad V_{3n} = 20.09 \times 10^{-3} \tag{8.22}$$

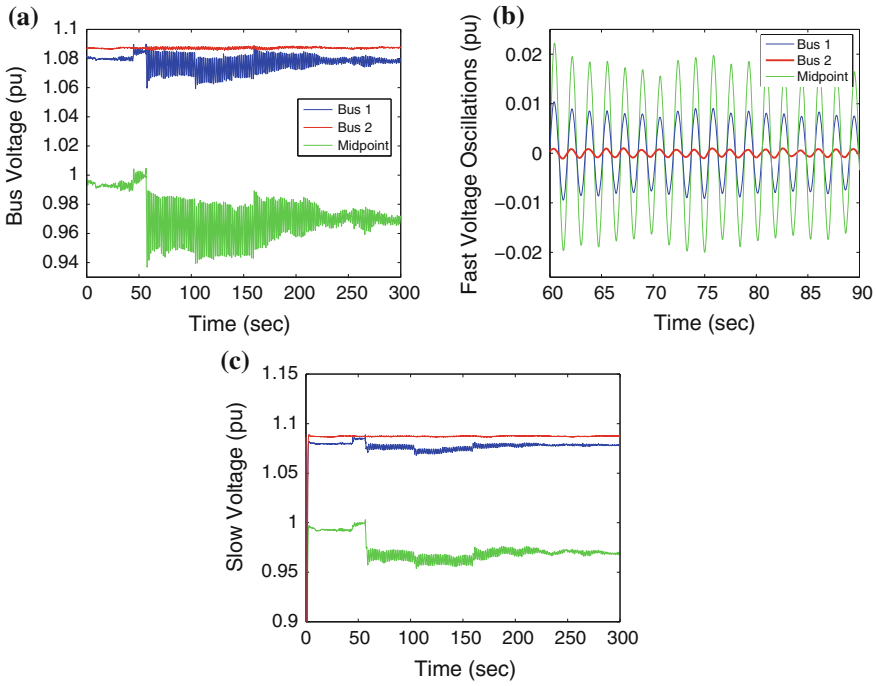

Fig. 8.3 Voltage oscillations in WECC transfer path 1. **a** Bus voltages in WECC transfer path 1. **b** Fast component of voltage magnitude. **c** Quasi-steady-state voltage magnitude

while $x_e = 0.077$ pu from least-squares estimation. Using the IME algorithm we get (in pu)

$$x_1 = 0.0121,\ x_2 = 0.0012,\ H_1 = 1050,\ H_2 = 134$$

The bus frequencies at the sending and receiving ends, their fast and slow components as well as their interarea components, used for estimating H_1 and H_2, are shown in Fig. 8.6. To verify the accuracy of the estimates, we also compare the interarea modal response of the voltage angles between the equivalent machines (as extracted via ERA) with the corresponding impulse response of the identified swing model. Figure 8.4c shows this comparison and confirms that the trajectories are sufficiently close to each other.

8.3 Star-Connected Three-Area System

Our system of interest in this section, namely a two-dimensional system with algebraic node(s), is motivated by the five-machine structure of the Pacific AC intertie model shown in Fig. 8.1a. The schematic circuit diagram of this system

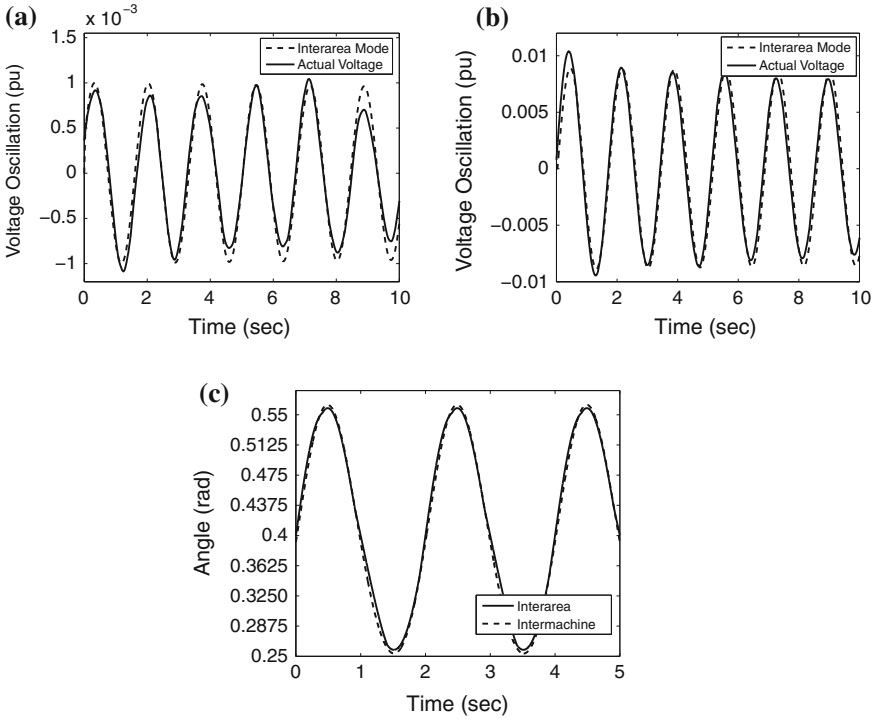

Fig. 8.4 Slow mode extraction for WECC transfer path 1 voltages. **a** Interarea oscillation at Bus 1. **b** Interarea oscillation at Bus 2. **c** Interarea versus intermachine oscillations

is shown in Fig. 8.7a. The basic problem formulation for reactance estimation for this system is similar to that in Sect. 8.2, i.e., using PMU measurements available from Buses 1, 2, 3 and 4, we need to solve for three unknown reactances, namely, $\sigma_i = x_{ei} + x_{Ti} + x'_{di}$, $i = 1, 2, 3$. Consider the star-connected three-machine equivalent of a three-area power system as shown in Fig. 8.7a. The classical model representation [18] of this three-machine system is shown in Fig. 8.7b. The system consists of three generators G_1, G_2, and G_3 with aggregated inertias H_1, H_2, and H_3 representing each coherent area [5], connected to Buses 1, 2 and 3 through transformers having equivalent reactances x_{T1}, x_{T2} and x_{T3}, respectively. The voltage phasors at Buses 1, 2, 3, and 4 are given as $\tilde{V}_i = V_i \angle \theta_i$, $i = 1, 2, 3, 4$, where $V\angle\theta$ denotes the polar representation $V\varepsilon^{j\theta}$. The transmission lines between Bus 4 and the other three buses are all assumed to be lossless, with line reactances x_{e1} between Buses 1 and 4, x_{e2} between Buses 2 and 4, and x_{e3} between Buses 3 and 4. The line current phasors shown in Fig. 8.7b are $\tilde{I}_i = I_i \angle \theta_{I_i}$, $i = 1, 2, 3$, with G_1 supplying power to G_2 and G_3, which act as loads. For the classical model representation, we denote the internal voltage phasors of the generators G_1, G_2, and G_3 as $\tilde{E}_i = E_i \angle \delta_i$, $i = 1, 2, 3$. The reactances connecting the generator internal voltages to Buses 1, 2, and 3 are given by

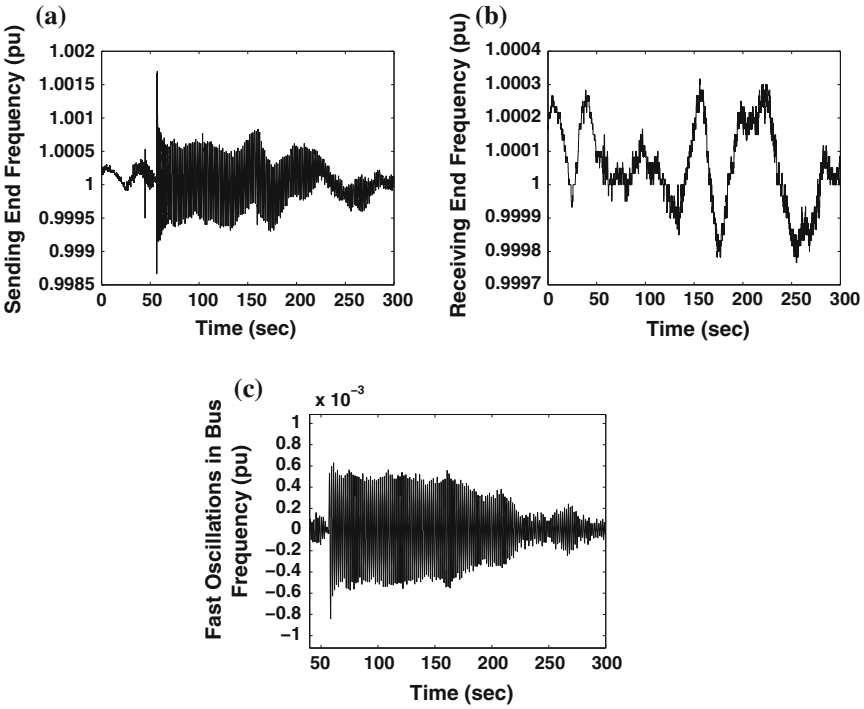

Fig. 8.5 Frequency oscillations in WECC transfer path 1. **a** Sending end frequency. **b** Receiving end frequency. **c** Fast component of sending end frequency

$$x_i = (x_{Ti} + x'_{di}), \qquad i = 1,\ 2,\ 3 \tag{8.23}$$

where x'_{d1}, x'_{d2}, and x'_{d3} are the direct-axis transient reactances of G_1, G_2, and G_3, respectively. For future use, we use the notations

$$\sigma_i = x_{ei} + x_i, \quad i = 1,\ 2,\ 3. \tag{8.24}$$

It should be noted that unlike the variant of the IME method considered in [20], here the generator G_2 is not necessarily a synchronous condenser, and, hence, there is no restrictive assumption about the equality of the voltage phase angles of Bus 2 and Bus 4.

The dynamic model of the three-machine system in Fig. 8.7b, neglecting damping, is given by

$$2H_1\,\ddot{\delta}_1 = P_{m1} - \frac{E_1 V_4}{\sigma_1}\sin(\delta_1 - \theta_4) \tag{8.25}$$

$$2H_2\,\ddot{\delta}_2 = P_{m2} - \frac{E_2 V_4}{\sigma_2}\sin(\delta_2 - \theta_4) \tag{8.26}$$

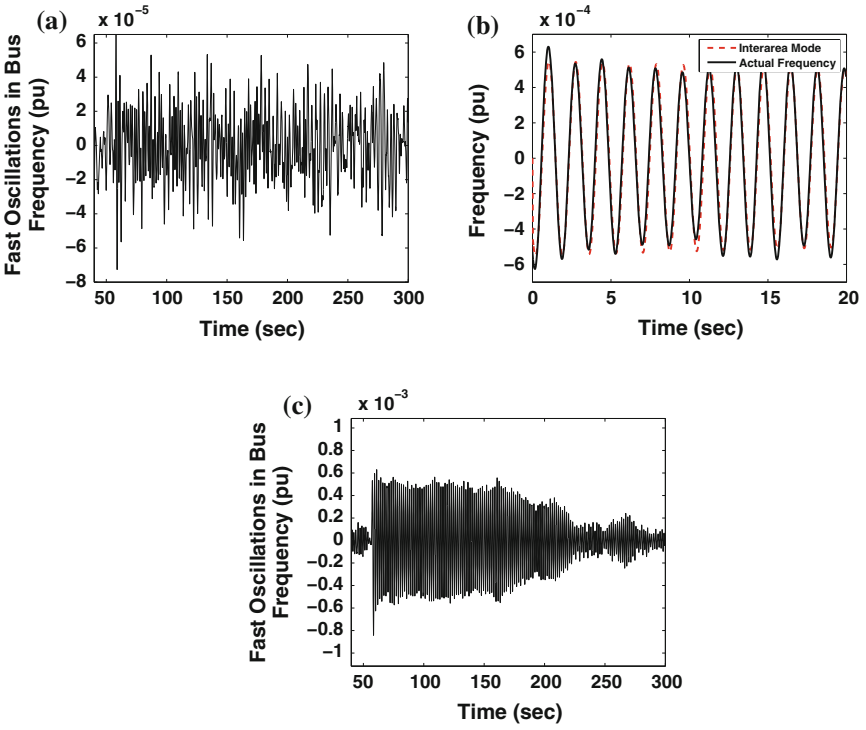

Fig. 8.6 Slow mode extraction for WECC transfer path 1 frequencies. **a** Fast component of receiving end frequency. **b** Interarea component of sending end frequency. **c** Interarea mode component of receiving end frequency

$$2H_3\,\ddot{\delta}_3 = P_{m3} - \frac{E_3 V_4}{\sigma_3}\sin(\delta_3 - \theta_4) \tag{8.27}$$

We assume that PMUs are located at Buses 1, 2, 3, and 4. Hence, high-sampling rate time-synchronized phasor variables $\tilde{V}_i$, $i = 1,\ 2,\ 3,\ 4$, and $\tilde{I}_i$, $i = 1,\ 2$, as a result of a disturbance are available. We pose the problem of finding the parameters of the model in Fig. 8.7b as follows.

Given the measured time-synchronized phasor variables V_1, θ_1, V_2, θ_2, V_3, θ_3, V_4, θ_4, I_1, θ_{I_1}, I_2, *and* θ_{I_2} *that exhibit a few cycles of interarea oscillations, and assuming that* E_1, E_2 *and* E_3 *are some constant values, compute* x_{e1}, x_{e2}, x_{e3}, E_1, δ_1, E_2, δ_2, E_3, δ_3, x_1, x_2, x_3, H_1, H_2 *and* H_3 *to completely characterize the dynamic behavior of the three-machine reduced system in* Fig. 8.7b.

Three of these quantities, namely, x_{e1}, x_{e2}, and x_{e3}, can readily be computed from the available bus voltages and currents using Ohm's law

$$jx_{e1} = \frac{\tilde{V}_1 - \tilde{V}_4}{\tilde{I}_1},\quad jx_{e2} = \frac{\tilde{V}_4 - \tilde{V}_2}{\tilde{I}_2},\quad jx_{e3} = \frac{\tilde{V}_4 - \tilde{V}_3}{\tilde{I}_3}. \tag{8.28}$$

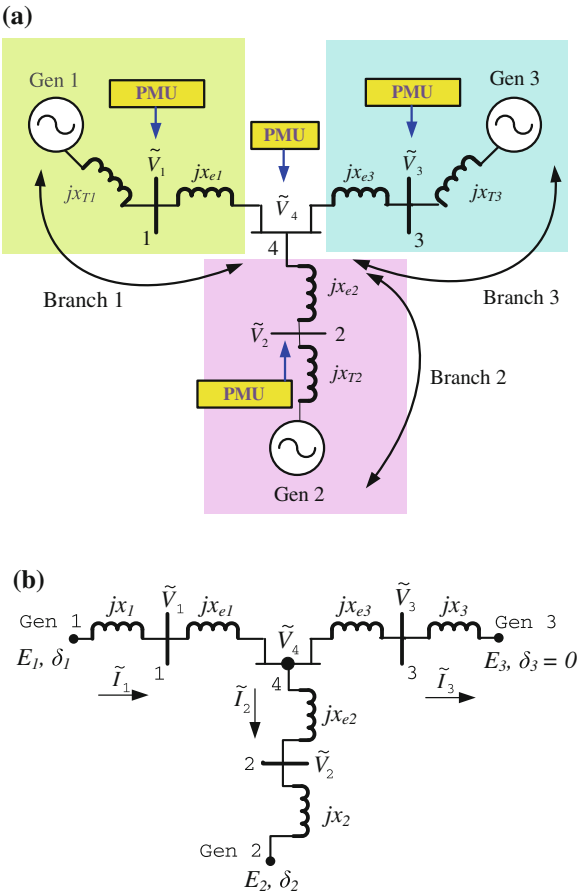

Fig. 8.7 Area aggregation of three-area power system. **a** Three-machine power system model. **b** Classical model representation

Moreover, if x_1, x_2, and x_3 are known, then the machine internal voltages can be computed from the bus voltages and the line currents. Thus, the problem reduces to the estimation of x_1, x_2, and x_3, as well as the inertias H_1, H_2, and H_3. In the following sections we develop techniques to estimate these six constant quantities.

Notations: A few notations used throughout the rest of the chapter are as follows. Subscripts R, L, and M, respectively, refer to quantities related to the right branch (between Generator 3 and Bus 4), left branch (between Bus 4 and Generator 1), and the middle branch (between Bus 4 and Generator 2) of the transfer path. The constant σ_{ij} is equal to σ_i/σ_j. The superscript i for any quantity refers to that quantity defined for Bus i, $(i = 1,\ 2,\ 3,\ 4)$. A small change in any of the measured variables, say an angle θ, over an existing equilibrium, is denoted as $\Delta\theta$ while $\Delta\theta^{ij}$ is equal

to $\Delta\theta^i/\Delta\theta^j$ where the superscript denotes the bus at which $\Delta\theta$ is measured. All quantities defined at the equilibrium are subscripted by 0.

8.3.1 Reactance Extrapolation: Branch 1

8.3.1.1 Step 1: Express $\tilde{V}_4$ as a Function of Generator Voltages

With $\tilde{E}_3$ as the reference, from circuit equations we can derive that

$$\tilde{V}_4 = \sigma(E_3 + \sigma_{31}\tilde{E}_1 + \sigma_{32}\tilde{E}_2) \tag{8.29}$$

where $\sigma \triangleq (\sigma_1\sigma_2)/(\sigma_1\sigma_2 + \sigma_2\sigma_3 + \sigma_3\sigma_1)$. We will use the expression in (8.29) for subsequent derivations in the following sections.

8.3.1.2 Step 2: Find Voltage Magnitude at an Arbitrary Point

Consider any point on the branch at a reactance jx away from Generator 3, which is taken as the reference node for this branch. The voltage phasor at this point can be written as

$$\tilde{V}_R = E_3(1 - a_3) + a_3\tilde{V}_4 \tag{8.30}$$

where $a_3 = x/\sigma_3 \in [0, 1]$. After a few calculations, it can be shown that the voltage magnitude at this point is

$$V_R(x, \delta_1, \delta_2) = \sqrt{\Sigma_R + \varpi_R(x, \delta_1, \delta_2)} \tag{8.31}$$

where Σ_R is a constant that is independent of δ_1 and δ_2,

$$\varpi(x, \delta_1, \delta_2) = \sum_{i=1}^{2} \alpha_{Ri}\cos(\delta_i) + \alpha_{R3}\cos(\delta_1 - \delta_2)$$

with $\alpha_{R1} = 2E_1E_3a_3(1 - a_3 + a_3\sigma)\sigma\sigma_{31}$, $\alpha_{R2} = 2E_2E_3a_3(1 - a_3 + a_3\sigma)\sigma\sigma_{32}$, and $\alpha_{R3} = 2E_1E_2a_3^2\sigma^2\sigma_{31}\sigma_{32}$.

8.3.1.3 Step 3: Form Normalized Voltage from a Small-Signal Perturbation

Consider a disturbance in the system, so that a small change in the voltage magnitude in (8.31), at the given point at time t, over a pre-disturbance equilibrium voltage $V_{R0}(x)$ can be written as

$$\Delta V_R(x,t) = \frac{P_{R1}(x)\Delta\delta_1(t) + P_{R2}(x)\Delta\delta_2(t)}{V_{R0}(x)} \tag{8.32}$$

where

$$P_{R1}(x) = -0.5(\alpha_{R3}\sin(\delta_{120}) + \alpha_{R1}\sin(\delta_{10}))$$
$$P_{R2}(x) = 0.5(\alpha_{R3}\sin(\delta_{120}) - \alpha_{R2}\sin(\delta_{20}))$$

and $\delta_{120} = \delta_{10} - \delta_{20}$. Next, we fix time at $t = t^*$, and denote $V_{Rn}(x) = \Delta V_R(x,t^*)V_{R0}(x)$, so that

$$V_{Rn}(x) = P_{R1}(x)\Delta\delta_1(t^*) + P_{R2}(x)\Delta\delta_2(t^*). \tag{8.33}$$

Because the normalized voltage can be measured at Buses 3 and 4 from PMU measurements following the disturbance, the quantities

$$V_n^3 \triangleq V_{Rn}(x_3), \quad V_n^4 \triangleq V_{Rn}(x_3 + x_{e3}) \tag{8.34}$$

are known. Denoting $P_{Ri}^3 = P_{Ri}(x_3)$ and $P_{Ri}^4 = P_{Ri}(x_3 + x_{e3})$, $i = 1, 2$, we can write

$$\frac{V_n^3}{V_n^4} = \frac{P_{R1}^3\Delta\delta_1(t^*) + P_{R2}^3\Delta\delta_2(t^*)}{P_{R1}^4\Delta\delta_1(t^*) + P_{R2}^4\Delta\delta_2(t^*)}. \tag{8.35}$$

The two hypothetical states $\Delta\delta_1(t^*)$ and $\Delta\delta_2(t^*)$ are unknown in (8.35). For the single interarea mode case of Sect. 8.2, this problem could be very easily bypassed as there was no term involving $\Delta\delta_2$, due to which the constant $\Delta\delta_1(t^*)$ could be cancelled in the numerator and the denominator of the right hand side of the equation, and the resulting nonlinear algebraic equation could be used toward solving for the unknown reactances. In other words, the *time–space separation property* is lost in (8.35) due to the extra interarea mode. To fix this problem, we next consider the change in the phase angles at Bus 3 and 4 as an extra degree of freedom, as follows.

8.3.1.4 Step 4: Derive the Change in Bus Phase Angles

The phase angle at any point on Branch 1, at a reactance x away from the Generator 3 node, is

$$\theta = \tan^{-1}\left(\frac{c_{R1}\sin(\delta_1) + c_{R2}\sin\delta_2}{c_{R3} + c_{R1}\cos(\delta_1) + c_{R2}\cos\delta_2}\right) \tag{8.36}$$

where $c_{R1} = E_1 a_3\sigma\sigma_{31}$, $c_{R2} = E_2 a_3\sigma\sigma_{32}$, and $c_{R3} = E_3(1 - a_3 + a_3\sigma)$. Using the fact that if $\theta = \tan^{-1}(\psi(\delta_1,\delta_2))$, then

$$\Delta\theta = \frac{1}{1+\psi^2}\left(\frac{\partial\psi}{\partial\delta_1}\Delta\delta_1 + \frac{\partial\psi}{\partial\delta_2}\Delta\delta_2\right)$$

it can be shown that a small change in the LHS of (8.36), at any time t, can be written as

$$\Delta\theta(x,t) = S_{R1}(x)\Delta\delta_1(t) + S_{R2}(x)\Delta\delta_1(t) \tag{8.37}$$

where S_{R1} and S_{R2} are given as

$$S_{R1}(x) = \frac{c_{R1}^2 + c_{R1}c_{R3}\cos(\delta_{10}) + c_{R1}c_{R2}\cos(\delta_{10}-\delta_{20})}{\vartheta_R(x)} \tag{8.38}$$

$$S_{R2}(x) = \frac{c_{R2}^2 + c_{R2}c_{R3}\cos(\delta_{20}) + c_{R1}c_{R2}\cos(\delta_{10}-\delta_{20})}{\vartheta_R(x)} \tag{8.39}$$

$$\begin{aligned}\vartheta_R(x) = {} & c_{R1}^2 + c_{R2}^2 + c_{R3}^2 + 2(c_{R1}c_{R3}\cos(\delta_{10}) + c_{R3}c_{R2}\cos(\delta_{20}) \\ & + c_{R2}c_{R1}\cos(\delta_{10}-\delta_{20}))\end{aligned} \tag{8.40}$$

8.3.1.5 Step 5: Formulate a Candidate Algebraic Equation

Fixing time at $t = t^*$, the fraction of the measured changes in the phase angles at Buses 3 and 4 in terms of the functions $S_{R1}(\cdot)$ and $S_{R2}(\cdot)$ defined at these respective bus locations, can then be written as

$$\frac{\Delta\theta^3}{\Delta\theta^4} = \frac{S_{R1}^3\Delta\delta_1(t^*) + S_{R2}^3\Delta\delta_1(t^*)}{S_{R1}^4\Delta\delta_2(t^*) + S_{R2}^4\Delta\delta_2(t^*)}. \tag{8.41}$$

Selecting t^* such that $\Delta\delta_1(t^*) \neq 0$ and $\Delta\delta_2(t^*) \neq 0$, (8.35) and (8.41) yield

$$\frac{V_n^3}{V_n^4} = \frac{P_{R1}^3(\Delta\theta^{34}S_{R2}^4 - S_{R2}^3) + P_{R2}^3(S_{R1}^3 - \Delta\theta^{34}S_{R1}^4)}{P_{R1}^4(\Delta\theta^{34}S_{R2}^4 - S_{R2}^3) + P_{R2}^4(S_{R1}^3 - \Delta\theta^{34}S_{R1}^4)}. \tag{8.42}$$

The LHS of (8.42) as well as the quantity $\Delta\theta^{34}$ on the RHS are measured while the other functions on the RHS are known nonlinear functions of $(x_1,\ x_2,\ x_3)$. Therefore, (8.42) serves as a feasible equation to solve for these three unknown reactances. The remaining two equations are constructed in the following sections using the measured phasor variables in Branches 2 and 3 of the network.

8.3.2 Reactance Extrapolation: Branch 2

Following an analysis similar to that used in Sect. 8.2.1, the normalized voltage at a point between Bus 4 and Generator 1, at a reactance x away from Bus 4,

$$V_{Ln}(x) = P_{L1}(x)\Delta\delta_1(t^*) + P_{L2}(x)\Delta\delta_2(t^*) \tag{8.43}$$

where

$$
\begin{aligned}
P_{Li} &= \frac{1}{2}(-\alpha_{L3}\sin(\delta_{10}-\delta_{20}) - \alpha_{Li}\sin(\delta_{i0})), \quad i = 1, 2\\
\alpha_{L1} &= 2E_1E_3a_1(1-a_1)\sigma + 2E_1E_3(1-a_1)^2\sigma^2\sigma_{31}\\
\alpha_{L2} &= 2E_2E_3(1-a_1)^2\sigma^2\sigma_{32}\\
\alpha_{L3} &= 2E_1E_2a_1(1-a_1)\sigma\sigma_{32} + 2E_1E_2(1-a_1)^2\sigma^2\sigma_{31}\sigma_{32}
\end{aligned}
$$

The equivalent of (8.42) for Branch 2 can then be written as

$$
\frac{V_n^1}{V_n^4} = \frac{P_{L1}^1(\Delta\theta^{14}S_{L2}^4 - S_{L2}^1) + P_{L2}^1(S_{L1}^1 - \Delta\theta^{14}S_{L1}^4)}{P_{L1}^4(\Delta\theta^{14}S_{L2}^4 - S_{L2}^1) + P_{L2}^4(S_{L1}^1 - \Delta\theta^{14}S_{L1}^4)} \tag{8.44}
$$

where the expressions for $S_{L1},\ S_{L2}$ are given as

$$
\begin{aligned}
S_{Li}(x) &= \left(c_{Li}^2 + c_{Li}c_{L3}\cos(\delta_{i0}) + c_{L1}c_{L2}\cos(\delta_{10}-\delta_{20})\right)/\vartheta_L(x), \quad i = 1, 2\\
\vartheta_L(x) &= c_{L1}^2 + c_{L2}^2 + c_{L3}^2 + 2c_{L3}\sum_{i=1}^{2}(c_{Li}\cos(\delta_{i0}) + c_{L2}c_{L1}\cos(\delta_{10}-\delta_{20}))\\
c_{L1} &= a_1E_1 + (1-a_1)E_1\sigma\sigma_{31}\\
c_{L2} &= E_2(1-a_1)\sigma\sigma_{32}, \quad c_{L3} = E_3(1-a_1)\sigma
\end{aligned}
$$

8.3.3 Reactance Extrapolation: Branch 3

For any point between Bus 4 and Generator 2, at a reactance x away from Bus 4, we have

$$
\frac{V_n^2}{V_n^4} = \frac{P_{M1}^2(\Delta\theta^{24}S_{M2}^4 - S_{M2}^2) + P_{M2}^2(S_{M1}^2 - \Delta\theta^{24}S_{M1}^4)}{P_{M1}^4(\Delta\theta^{24}S_{M2}^4 - S_{M2}^2) + P_{M2}^4(S_{M1}^2 - \Delta\theta^{24}S_{M1}^4)} \tag{8.45}
$$

where

$$
\begin{aligned}
P_{Mi} &= \frac{1}{2}(-\alpha_{M3}\sin(\delta_{10}-\delta_{20}) - \alpha_{Mi}\sin(\delta_{i0})), \quad i = 1, 2\\
\alpha_{M1} &= 2E_1E_3(1-a_2)^2\sigma^2\sigma_{31}\\
\alpha_{M2} &= 2E_2E_3a_2(1-a_2)\sigma + 2E_2E_3(1-a_2)^2\sigma^2\sigma_{32}\\
\alpha_{M3} &= 2E_1E_2a_2(1-a_2)\sigma\sigma_{31} + 2E_1E_2(1-a_2)^2\sigma^2\sigma_{31}\sigma_{32}
\end{aligned}
$$

with $a_2 = x/\sigma_2$, and the expressions for S_{M1} and S_{M2} are given as

$$S_{Mi}(x) = (c_{Mi}^2 + c_{Mi}c_{M3}\cos(\delta_{i0}) + c_{M1}c_{M2}\cos(\delta_{10} - \delta_{20}))/\vartheta_M(x), \quad i = 1, 2$$

$$\vartheta_M(x) = c_{L1}^2 + c_{M2}^2 + c_{M3}^2 + 2c_{M3}\sum_{i=1}^{2}(c_{Mi}\cos(\delta_{i0}) + c_{M2}c_{M1}\cos(\delta_{10} - \delta_{20}))$$

$$c_{M1} = (1 - a_2)E_1\sigma\sigma_{31}$$

$$c_{M2} = a_2E_2 + E_2(1 - a_2)\sigma\sigma_{32}, \quad c_{M3} = E_3(1 - a_2)\sigma$$

Equations (8.42), (8.44), and (8.45) can now be used to solve for the three unknowns x_1, x_2, and x_3 using the measurements of the bus voltage magnitudes and phase angles.

8.3.4 Machine Inertia Estimation

To solve for the three inertias H_1, H_2, and H_3 we need three equations. The first two equations are given from the expressions for the frequencies of the two interarea modes. For this we consider the electromechanical swing equations for the three machines, given by (8.25–8.27). However, we should note that in these equations, the two variables V_4 and θ_4 are not constants, but functions of the generator angles according to (8.29). Considering this fact, we next linearize (8.25–8.27) about the post-disturbance equilibrium, to get a linear equation of the form

$$\ddot{\delta} = \mathscr{H}^{-1}\mathscr{A}\delta \tag{8.46}$$

where $\delta = \text{col}(\delta_1, \delta_2, \delta_3)$, $\mathscr{H} = \text{diag}(2H_1, 2H_2, 2H_3)$ and $\mathscr{A}$ is a 3×3 matrix, whose entries are all known once the three reactances x_1, x_2, and x_3 are solved for, using the method described in Sects. 8.3.1–8.3.3. To find the interarea dynamics, we next fix δ_3 as the reference angle, and define the relative angular separations as

$$\delta_{13} = \delta_1 - \delta_3, \quad \delta_{23} = \delta_2 - \delta_3. \tag{8.47}$$

Consider $\mathscr{A}_1$, $\mathscr{A}_2$ and $\mathscr{A}_3$ to be the first, second and third rows of the matrix $\mathscr{A}$ in (8.46), respectively. It can be readily seen that

$$\ddot{\delta}_{13} = (\bar{\mathscr{A}_1} - \bar{\mathscr{A}_3})\delta, \quad \ddot{\delta}_{23} = (\bar{\mathscr{A}_2} - \bar{\mathscr{A}_3})\delta \tag{8.48}$$

where $\bar{\mathscr{A}_1} = \mathscr{A}_1/(2H_1)$, $\bar{\mathscr{A}_2} = \mathscr{A}_2/(2H_2)$, $\bar{\mathscr{A}_3} = \mathscr{A}_3/(2H_3)$. Also, we have

$$\begin{bmatrix} \delta_{13} \\ \delta_{23} \end{bmatrix} = \begin{bmatrix} 1 & 0 & -1 \\ 0 & 1 & -1 \end{bmatrix}\delta. \tag{8.49}$$

Combining (8.48) and (8.49) we can write

$$\begin{bmatrix} \ddot{\delta}_{13} \\ \ddot{\delta}_{23} \end{bmatrix} = \underbrace{\begin{bmatrix} \bar{\mathscr{A}}_1 - \bar{\mathscr{A}}_3 \\ \bar{\mathscr{A}}_2 - \bar{\mathscr{A}}_3 \end{bmatrix} \begin{bmatrix} 1 & 0 & -1 \\ 0 & 1 & -1 \end{bmatrix}^{+}}_{\Upsilon} \begin{bmatrix} \delta_{13} \\ \delta_{23} \end{bmatrix}. \tag{8.50}$$

Denoting $\mathscr{A}_i = [a_{i1}\, a_{i2}\, a_{i3}]$, $i = 1, 2, 3$, the structure of the 2×2 matrix Υ is given as

$$\Upsilon = \begin{bmatrix} \frac{2a_{11} - a_{12} - a_{13}}{H_1} - \frac{2a_{31} - a_{32} - a_{33}}{H_3} & \frac{2a_{12} - a_{11} - a_{13}}{H_1} - \frac{2a_{32} - a_{31} - a_{33}}{H_3} \\ \frac{2a_{21} - a_{22} - a_{23}}{H_2} - \frac{2a_{31} - a_{32} - a_{33}}{H_3} & \frac{2a_{22} - a_{21} - a_{23}}{H_2} - \frac{2a_{32} - a_{31} - a_{33}}{H_3} \end{bmatrix} \tag{8.51}$$

Let the entries of this matrix be denoted as υ_{ij} where i is the row index and j is the column index. Then it follows that the eigenvalues of Υ are given as

$$\lambda_{1,2} = \frac{\upsilon_{11} + \upsilon_{22} \pm \sqrt{(\upsilon_{11} - \upsilon_{22})^2 + 4\upsilon_{12}\upsilon_{21}}}{2}, \tag{8.52}$$

and the respective eigenvectors e_1 and e_2 are given as solutions to the equations

$$\Upsilon e_1 = \lambda_1 e_1, \quad \Upsilon e_2 = \lambda_2 e_2. \tag{8.53}$$

It is clear from (8.51) that λ_1, λ_2, e_1 and e_2 are all functions of H_1, H_2, and H_3. The frequencies of the interarea oscillations can be measured from the difference signals $(\theta_1 - \theta_2)$ and $(\theta_2 - \theta_3)$ using modal analysis (such as ERA or a subspace identification algorithm). Say these frequencies (in Hz) are f_{s1} and f_{s2}, and the computed respective eigenvectors are φ_{s1} and φ_{s2}. Then we can write

$$f_{s1} = \frac{1}{2\pi}\sqrt{\lambda_1}, \quad \varphi_{s1} = e_1 \tag{8.54}$$

$$f_{s2} = \frac{1}{2\pi}\sqrt{\lambda_2}, \quad \varphi_{s2} = e_2. \tag{8.55}$$

Either (8.54) or (8.55) may be used as two equations for solving for the three unknown inertias as f_{s1}, f_{s2}, φ_{s1} and φ_{s2} are known quantities. An important point to note here is that although the three-area system under consideration contains two interarea modes of oscillation it is sufficient to consider the participation of only one of these modes in the PMU measurements for solving the EIME problem. For example, the estimation of the unknown reactances, as in (8.25), (8.33), and (8.34), involves the elimination of one of the interarea modes by considering the simultaneous measurement of voltage magnitudes and phase angles. Similarly, the estimation of the unknown inertias in (8.43–8.44) requires the modal decomposition of only one interarea mode. The resulting EIME algorithm, as summarized in Fig. 8.9, therefore, does not depend on which modal component out of the two is selected from the

PMU measurements for solving for the unknown parameters. The idea is illustrated in Fig. 8.8.

The third equation is given by the law of conservation of angular momentum, which can be simply written as

$$H_1\omega_1 + H_2\omega_2 + H_3\omega_3 = 0 \tag{8.56}$$

where ω_i is the angular speed (rad/s) of the ith generator ($i = 1,\ 2,\ 3$). These speeds are not measured, but can be estimated from the measured bus frequencies ν_1, ν_2, and ν_3 at Buses 1, 2, and 3, respectively, as discussed in [20]. The basic methodology to achieve this is to express the voltage phasor $\tilde{V}$ at any point in terms of $E_1\angle\delta_1$, $E_2\angle\delta_2$, and $E_3\angle\delta_3$ and the reactance x with respect to some chosen reference; then calculate the phasor angle

$$\theta = \tan^{-1}(\mathrm{Im}(\tilde{V})/\mathrm{Re}(\tilde{V})) \tag{8.57}$$

and compute the time derivative of θ as a function of x, ω_1, ω_2 and ω_3. For the three-machine system of Fig. 8.7b, after some calculations it can be shown that the frequency at any point on the path is given by

$$\nu(x, \delta_1, \delta_2, \delta_3) = \frac{\Pi_1(x, \delta_1, \delta_2, \delta_3)}{\Pi_2(x, \delta_1, \delta_2, \delta_3)} \tag{8.58}$$

where the functions $\Pi_1(\cdot)$ and $\Pi_2(\cdot)$ are given as

$$\begin{aligned}\Pi_1(x, \delta_1, \delta_2, \delta_3) = \omega_1 &\left[n_1^2E_1^2 + n_1n_2E_1E_2\cos(\delta_1 - \delta_2) + n_1n_3E_1E_3\cos(\delta_1 - \delta_3)\right] \\ + \omega_2 &\left[n_2^2E_2^2 + n_2n_3E_2E_3\cos(\delta_2 - \delta_3) + n_2n_1E_2E_1\cos(\delta_2 - \delta_1)\right] \\ + \omega_3 &\left[n_3^2E_3^2 + n_3n_1E_3E_1\cos(\delta_3 - \delta_1) + n_3n_2E_3E_2\cos(\delta_3 - \delta_2)\right]\end{aligned}$$

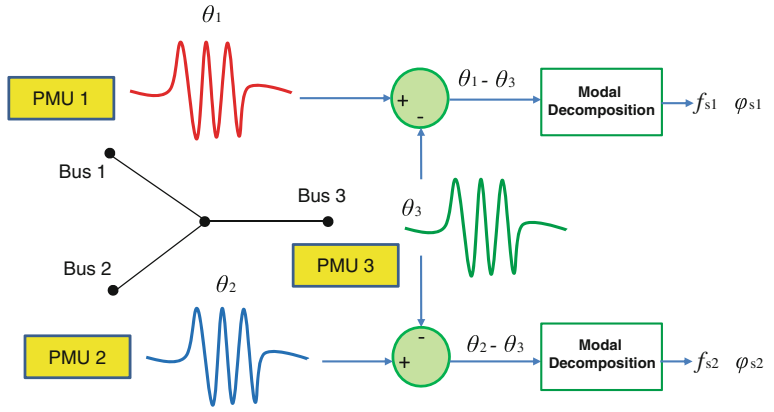

Fig. 8.8 Choice of interarea mode for computation of unknown machine inertias

A Summary of the EIME Algorithm

1. Consider the three-machine system in Figure 8.1(b). Following a disturbance in the system, measure the voltage phasors $\tilde{V}_1$, $\tilde{V}_2$, $\tilde{V}_3$, and $\tilde{V}_4$ at Buses 1, 2, 3 and 4, respectively, and the currents $\tilde{I}_1$, $\tilde{I}_2$ and $\tilde{I}_3$.
2. Calculate the line reactances x_{e1}, x_{e2}, and x_{e3} using (8.28).
3. Measure the amplitudes of oscillation in the magnitudes of $\tilde{V}_i$ ($i = 1,..,4$) at one particular instant of time, for example, when they reach a peak simultaneously.
4. Multiply the measured amplitudes with the respective steady-state values of the voltage waveforms to get the normalized voltage amplitudes at these four buses.
5. Measure the amplitudes of oscillation in the phase angles of $\tilde{V}_i$ ($i = 1,..., 4$) at the same instant of time.
6. Solve for x_1, x_2, and x_3 using equations (8.42), (8.44), and (8.45).
7. Calculate the constant generator internal voltages using the extrapolated reactances, the bus voltages, and the line currents.
8. Calculate the inter-area swing frequency (eigenvalue) and the corresponding eigenvector for any one of the two inter-area modes from the measured bus voltages using modal decomposition such as ERA.
9. Use the extrapolated system parameters and the inter-area frequencies to get two equations in the machine inertias using (8.51), (8.54), and (8.55).
10. Use the measured bus frequencies ν_1 and ν_2 to estimate ω_1 and ω_2 using (8.58) and (8.62).
11. Compute H_1, H_2 and H_3 from Step 9 and equation (8.56) .

Fig. 8.9 A summary of the EIME algorithm

$$\Pi_2(x, \delta_1, \delta_2, \delta_3) = n_1^2 E_1^2 + n_2^2 E_2^2 + n_3^2 E_3^2 + 2\Big[n_1 n_2 E_1 E_2 \cos(\delta_1 - \delta_2) + n_2 n_3 E_2 E_3 \cos(\delta_2 - \delta_3) + n_3 n_1 E_3 E_1 \cos(\delta_3 - \delta_1)\Big]$$

with n_1, n_2, and n_3 defined as follows. The references for measuring x are fixed at Bus 4 for Branches 1 and 3, and at Generator 1 for Branch 1. Also, as defined before, a_1, a_2, and a_3 denote the normalized reactances (or equivalently distances) measured along Branches 1, 2, and 3, respectively, from their respective reference points:

1. *Branch* 1: Between Bus 4 and Generator 3

$$n_1 = \sigma\sigma_{31}(1 - a_3), \quad n_2 = \sigma\sigma_{32}(1 - a_3), \quad n_3 = \sigma(1 - a_3) + a_3 \tag{8.59}$$

2. *Branch* 2: Between Generator 1 and Bus 4

$$n_1 = 1 - a_1 + a_1\sigma\sigma_{31}, \quad n_2 = a_1\sigma\sigma_{32}, \quad n_3 = a_1\sigma \tag{8.60}$$

3. *Branch* 3: Between Bus 4 and Generator 2

$$n_1 = \sigma\sigma_{31}(1-a_2), \quad n_2 = \sigma\sigma_{32}(1-a_2)+a_2, \quad n_3 = \sigma(1-a_2). \tag{8.61}$$

Therefore, the frequencies at Buses 1, 2, and 3 can be expressed as

$$\begin{aligned} \nu_1 &= \frac{\Pi_1(x_1,\delta_1,\delta_2,\delta_3)}{\Pi_2(x_1,\delta_1,\delta_2,\delta_3)}, \quad \nu_2 = \frac{\Pi_1(x_{e2},\delta_1,\delta_2,\delta_3)}{\Pi_2(x_{e2},\delta_1,\delta_2,\delta_3)}, \\ \nu_3 &= \frac{\Pi_1(x_{e3},\delta_1,\delta_2,\delta_3)}{\Pi_2(x_{e3},\delta_1,\delta_2,\delta_3)}. \end{aligned} \tag{8.62}$$

Since the bus frequencies are measured (or derived by passing the bus angles through high-pass filters), ν_1, ν_2, and ν_3 are known at any chosen time instant. Also, once x_1 and x_2 are identified, E_i and δ_i ($i = 1, 2, 3$) can be calculated for the same time instant, and hence, the three equations in (8.62) can be solved for ω_1, ω_2, and ω_3. The solution of H_1 and H_2 then follows from (8.54) or (8.55) and (8.56). The entire algorithm is described step-by-step in Fig. 8.9.

8.3.5 Reduced-Order Modeling of Pacific AC Intertie

This transfer path is a large group of generators supplying power via a 1,200-mile transmission system to a large load center with an intermediate generation cluster attached to the path, as shown in Fig. 8.1a. Figure 8.10a shows the bus voltage magnitudes at 6 buses on the transfer path, with Buses 1, 2, and 3 being the sending end, receiving end, and the intermediate generation bus, respectively. Figures 8.10b and c show the separated fast and slow components for each of the six bus voltages. As both the sending and receiving ends have a large group of generators, a significant number of swing modes contributes to the oscillations in Fig. 8.10b, only one of which is the interarea mode. The oscillation due to this mode is dominant in all six voltages. We apply the eigensystem realization algorithm (ERA) to extract the modes and their mode shapes in the time response of the voltage oscillations, starting from $t = 62$ s to $t = 80$ s. ERA shows that over this chosen time-window of 18 s, the oscillations can be approximated by a dominant interarea mode of 0.404 Hz. Figure 8.11 shows the 0.404 Hz mode components superimposed on the individual voltage magnitude oscillations at Buses 1, 2, and 3. Similar figures can be drawn for the remaining buses.

The magnitude V_{im} (in pu) of the interarea mode components of the i^{th} bus voltage ($i = 1, 2, 3$) can be obtained from the approximated (dotted) voltage responses in Fig. 8.11a, b, and c at a fixed point of time. Choosing this fixed time point at $t = 4$ s, where the positive peak of the second cycle occurs, we get (in pu)

$$V_{1m} = 1.897 \times 10^{-3}, \quad V_{2m} = 2.615 \times 10^{-3}, \quad V_{3m} = 5.206 \times 10^{-3} \tag{8.63}$$

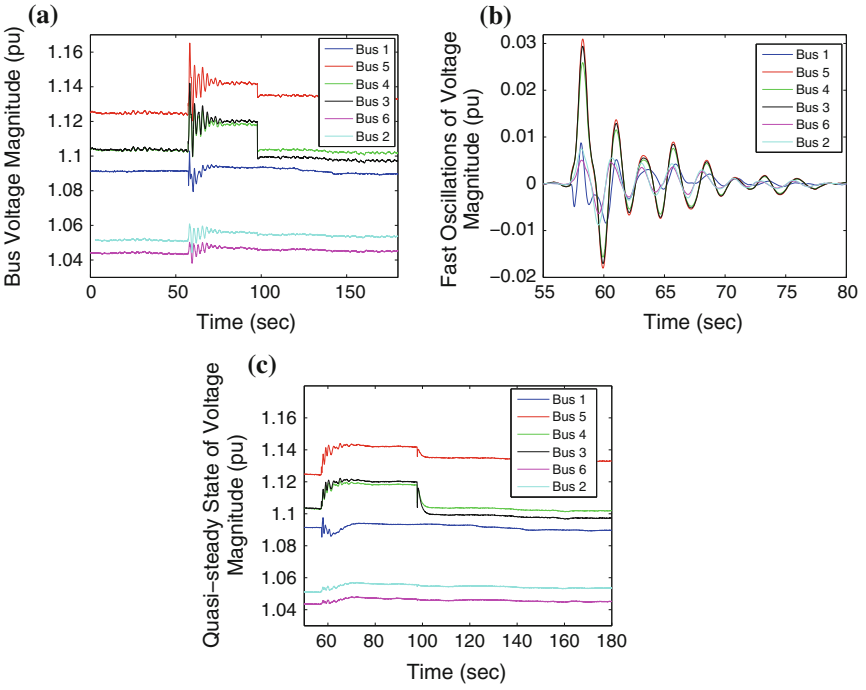

Fig. 8.10 Bus voltage magnitudes for WECC transfer path 2. **a** Bus 1 voltage. **b** Bus 2 voltage. **c** Bus 3 voltage

As the signals used for mode extraction start from $t = 62\,\text{s}$ in the original time response of Fig. 8.10a, the chosen fixed time-point is equal to $t = 66\,\text{s}$. The quasi-steady-state values $V_{i\text{ss}}$ of the i^{th} bus voltage ($i = 1, ..., 6$) are obtained from the slow parts of the voltages shown in Fig. 8.10c at the pre-disturbance time instant as

$$V_{1\text{ss}} = 1.0903, \quad V_{2\text{ss}} = 1.046, \quad V_{3\text{ss}} = 1.1234 \tag{8.64}$$

Therefore, the normalized voltage amplitudes are (in pu)

$$V_{1n} = 2.0683 \times 10^{-3}, \quad V_{2n} = 2.7353 \times 10^{-3}, \quad V_{3n} = 5.8482 \times 10^{-3} \tag{8.65}$$

Applying the IME algorithm from (8.42), (8.44), and (8.45), we obtain

$$x_1 = 0.00411, \quad x_2 = 0.00655 \tag{8.66}$$

where x_1 (in pu) is the sum of the aggregated transformer reactance and direct-axis transient reactance of the sending end equivalent generator, and x_2 (in pu) is that of the receiving end equivalent generator. The Jacobian curve is shown in Fig. 8.12.

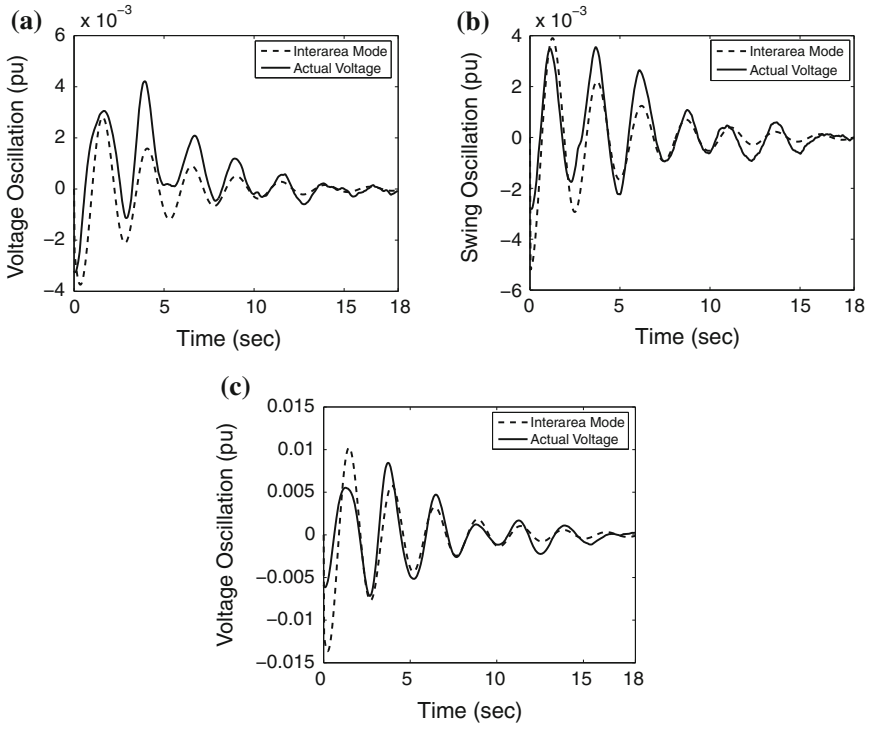

Fig. 8.11 Interarea bus voltage magnitudes for WECC transfer path 2. **a** Bus 1 voltage. **b** Bus 2 voltage. **c** Bus 3 voltage

From the curve, it can be easily seen that oscillations are much more damped on the right half of the transfer path due to the high loading effect on this side.

The inertia constant (pu) between the two dominant generators is approximately $H = 810\,\text{pu}$. However, the voltage droop at the *star point* is not very significant, which indicates that the third generator does not produce a strong impact on the voltage profile. The Jacobian fit without the effect of this extra interarea mode is shown in Fig. 8.12 as the dashed curve.

8.4 Multi-Modal Interarea Equivalents

In this section we generalize the idea presented in Sect. 8.3 to a multi-area system where each area is *directly* connected to its neighboring set of areas without the existence of any algebraic bus. As before, we represent each area by an equivalent synchronous machine, and assume that the equivalent topology of the system is known. Unlike Sect. 8.3 the advantage here is that we do not need to compute the voltage phasor at any algebraic bus, and can apply the IME algorithm of Sect. 8.2

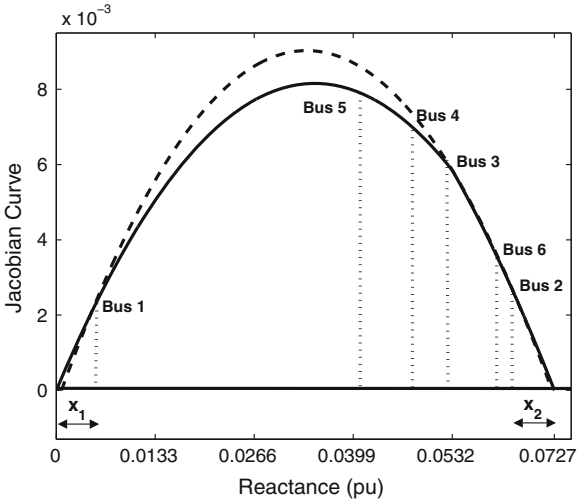

Fig. 8.12 Jacobian curves for Pacific AC Intertie—with second interarea mode (*solid*), without second interarea mode (*dashed*)

directly to every pair of connected areas in a *decentralized* fashion provided that the contribution of every slow mode is retained in the bus measurements. The idea is illustrated by the three-machine system in Fig. 8.13a, where each of the three machines G_1, G_2, and G_3, connected to each other by a ring topology, represent the equivalent of an area consisting of multiple local machines. PMUs are assumed to be installed at the terminal buses of each machine.

The swing dynamics of the equivalent system is given by

$$2H_1\ddot{\delta}_1 = P_{m1} - \frac{E_1E_2}{x_{12}}\sin(\delta_1 - \delta_2) - \frac{E_1E_3}{x_{13}}\sin(\delta_1 - \delta_3) \tag{8.67}$$

$$2H_2\ddot{\delta}_2 = P_{m2} - \frac{E_2E_3}{x_{23}}\sin(\delta_2 - \delta_3) - \frac{E_2E_1}{x_{12}}\sin(\delta_2 - \delta_1) \tag{8.68}$$

$$2H_3\ddot{\delta}_3 = P_{m3} - \frac{E_3E_1}{x_{13}}\sin(\delta_3 - \delta_1) - \frac{E_3E_2}{x_{23}}\sin(\delta_3 - \delta_2) \tag{8.69}$$

where P_{mi} is the effective mechanical power input to the i^{th} area, and x_{ik} is the total reactance connecting the internal node of the i^{th} and k^{th} equivalent machines. However, because each area may contain internal loads, we assume the line currents across each transfer path to be different, namely $\tilde{I}_1$, $\tilde{I}_2$, and $\tilde{I}_3$. All three currents are available from the respective PMU measurements. The equivalent transmission line reactances can be calculated from the bus voltage and current measurements using Ohm's law, while the total reactance between the internal node of any machine and any of the terminal buses needs to be estimated using IME. Assuming a classical model for synchronous machines, this total reactance is assumed to be the sum of the

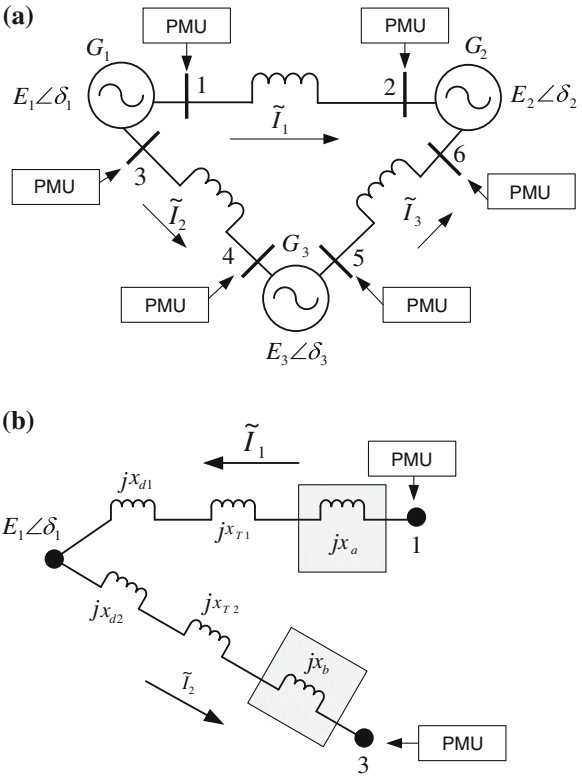

Fig. 8.13 Equivalent circuit of a multimodal power system. **a** 2-dimensional system. **b** Reactance matching

direct-axis transient reactance and the transformer reactance, namely, $(x'_{d_{ij}} + x_{T_{ij}})$, for the i^{th} area connected to the j^{th} terminal bus. Because Kirchoff's law holds for each transfer path independently, IME can be applied to each pair of machines to calculate this reactances irrespective of the other paths. However, two important points must be taken into consideration before applying IME:

1. Because the internal node of each machine is the point of common coupling between any two neighboring transfer paths, we must make sure that this internal voltage computed independently from the reactance estimates of each path must match with each other. For example, using Kirchoff's law at the internal node of G_1, first for transfer path 1–2 and then for the path 1–3, we get, respectively,

$$E_1 = |\tilde{V}_1 + j(x'_{d_{11}} + x_{T_{11}})\,\tilde{I}_1|, \quad E_1 = |\tilde{V}_2 + j(x'_{d_{13}} + x_{T_{13}})\,\tilde{I}_2|, \quad (8.70)$$

   where, $\tilde{V}_i$ and $\tilde{I}_i$ are available from PMU measurements and the reactances are estimated independently using IME. Because the LHS may not necessarily match

for both equations, we, therefore, add two fictitious reactances jx_a and jx_b on each side, and tune them till we obtain the same value of E_1. The same approach applies to the internal reactance of all other areas. Physically speaking, this may be thought of as a variable reactance that matches the internal angle of each equivalent machine at the cost of decentralized estimation of the area parameters. These fictitious reactances are illustrated in Fig. 8.13b.

2. Decentralization of IME, however, should not neglect the basic fact that the dynamics of the three machines are coupled to each other, and, therefore, all the bus measurements used for estimating the reactances and inertias must contain the contribution of each and every slow mode of oscillation. This can be easily accounted for from the fundamental principle behind coherency and aggregation [5]. For example, to obtain an analytical expression for the fast and slow oscillation dynamics, one may define the slow or aggregate variable for the k^{th} area to be the so-called center of inertia angle for that area, namely

$$y_k \triangleq \frac{\sum_{i=1}^{n_k} H_i^k \delta_i^k}{\sum_{i=1}^{n_k} H_i^k}, \quad k = 1, 2, ...r \tag{8.71}$$

where δ_i^k and H_i^k are, respectively, the i^{th} machine angle and inertia in the k^{th} area, n_k is the total number of machines in the k^{th} area, and r is the total number of areas. Similarly, the fast variable for the k^{th} area can be defined as

$$z_{k,i} \triangleq \delta_i^k - \delta_1^k, \quad i = 1, 2, ...n_k, \quad k = 1, 2, ...r. \tag{8.72}$$

The time-scale separation between the fast and slow oscillations can then be expressed explicitly in the singular perturbed form

$$\frac{\mathrm{d}y}{\mathrm{d}t_s} = A_{11}y + A_{12}z, \quad \varepsilon\frac{\mathrm{d}z}{\mathrm{d}t_s} = A_{21}y + A_{22}z \tag{8.73}$$

where $\varepsilon \ll 1$ is a small parameter, and the exact expressions for the four state matrices can be found in [5]. Assuming $\varepsilon \approx 0$, the effective swing dynamics for the interarea oscillations can then be written as:

$$\frac{\mathrm{d}y}{\mathrm{d}t_s} = (A_{11} - A_{12}\,A_{22}^{-1}\,A_{21})y. \tag{8.74}$$

Because the matrix $(A_{11} - A_{12}\,A_{22}^{-1}\,A_{21})$ is not necessarily block-diagonal, it is evident that the interarea oscillation modes are not necessarily decoupled. In other words, the bus voltage oscillations available from the PMUs at each terminal bus must retain the cumulative contribution of all slow modes. This can also be seen from the time-domain representation of the i^{th} bus voltage, namely

$$V_k = \left(\sum_{i=1}^{n-1} R_i e^{-\sigma_i t} (\sin(\omega_i t + \phi_i) + \cos(\omega_i t + \phi_i)) \right)_k \tag{8.75}$$

where n is the total number of machines in the system. However, the RHS of (8.75) contains the contribution of both local and interarea modes, only the two slowest of which will give the contribution of the interarea oscillations in our example of interest.

The net interarea component of V_k can then be written as

$$\begin{aligned} V_k^s = \Big(& R_1 e^{-\sigma_1 t} (\sin(\omega_1 t + \phi_1) + \cos(\omega_1 t + \phi_1)) \\ & + R_2 e^{-\sigma_2 t} (\sin(\omega_2 t + \phi_2) + \cos(\omega_2 t + \phi_2)) \Big)_k \end{aligned} \tag{8.76}$$

where ω_1 and ω_2 are the two slow frequencies. These two frequencies and their corresponding residues and damping factors in (8.76) can be easily computed by applying modal decomposition to the bus voltage measurement V_i, some common methods including the ERA, Prony analysis, and Matrix Pencil. Once V_k^s is extracted for $k = 1, 2, \ldots, 6$, these voltages can then be used for calculating the internal reactances of each area (for each connection) via IME in exactly the same way as in Sect. 8.2 for each pair of machines. The same idea applies to the bus frequencies for estimating the equivalent machine inertias. One interesting observation, however, is that the machines do not necessarily have unique inertias, but have as many distinct inertias as the degree of that node, each representing the effective *weight* of that area contributing to the oscillation for each respective transfer path that the machine is connected to. A schematic of the spatial variation of voltage at any fixed point of time for this three-machine system is shown in Fig. 8.14.

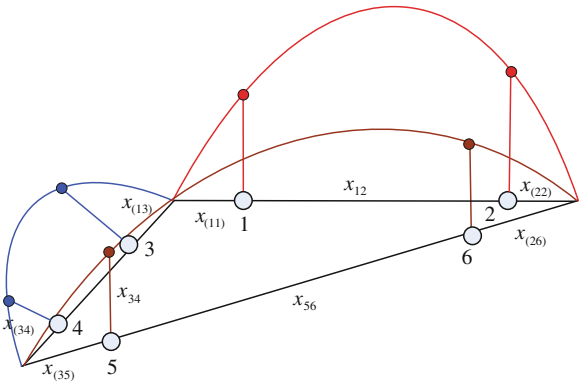

Fig. 8.14 Spatial variation of voltage for 2-dimensional system

8.5 Transient Stability Assessment Using Energy Functions

In this section we show how the reduced-order models developed in Sect. 8.2 can be exploited to formulate performance metrics for transient and damping stability assessment of two-area power systems. We develop the concepts to compute energy functions using phasor data to assess the stability margin of power transfer paths. Consider a two-machine equivalent system as in Fig. 8.2b, and let its post-fault equilibrium angle be δ_{op}. The energy function V_E of the system can be expressed in the form

$$V_E = V_{\text{PE}} + V_{\text{KE}} \tag{8.77}$$

where the potential energy and the kinetic energy are given by

$$V_{\text{PE}} = \frac{E_1 E_2}{x'_e}\Big(\cos(\delta_{op}) - \cos(\delta) + \sin(\delta_{op})(\delta_{op} - \delta)\Big) \tag{8.78}$$

$$V_{\text{KE}} = \frac{1}{2}(2H)\Omega\omega^2 = H\Omega\omega^2. \tag{8.79}$$

It should be noted that by virtue of the IME algorithm, the energy function (8.77) can be computed in terms of the machine angles and voltages extrapolated from the bus measurements. However, the bus voltages contain high-frequency local modes as well as slower interarea modes. These fast and slow components need to be separated before using the voltages to construct the energy function. We call the filtered slow component of the voltages as the quasi-steady-states $\bar{V}_1$ and $\bar{V}_2$. In real time, the post-fault equilibrium angle δ_{op} or θ_{op} is not fixed either, but rather time varying, due to turbine-generator governing and other generation and load changes. Thus we can write

$$\delta = \hat{\delta} + \delta_{\text{qss}} \tag{8.80}$$

where $\hat{\delta}$ and δ_{qss} are respectively the swing component and the quasi-steady-state components of δ. We need to extract the quasi-steady-state value δ_{qss} in order to approximate the post-disturbance equilibrium angle used in the potential energy function (8.78). Based on this, we propose the transient swing energy function

$$\hat{V}_E(t) = \hat{V}_{\text{KE}}(t) + \hat{V}_{\text{PE}}(t) \tag{8.81}$$

to model the energy due to the dominant interarea mode, where

$$\hat{V}_{\text{PE}} = \frac{\bar{E}_1 \bar{E}_2}{x'_e}\left(\cos(\delta_{\text{qss}}) - \cos(\delta) + \sin(\delta_{\text{qss}})(\delta_{\text{qss}} - \delta)\right) \tag{8.82}$$

$$\hat{V}_{\text{KE}}(t) = H\Omega\omega(t)^2 \tag{8.83}$$

where δ_{qss} is obtained in practice by bandpass filtering the δ measurement.

We next illustrate the construction of (8.81–8.83) using a disturbance event in the two-area WECC transfer path discussed in Sect. 8.2. After applying the IME algorithm to the bus measurements and extrapolating to the machine internal nodes, the time variations of the machine angular separation and frequency differences are calculated, and plotted, respectively, in Fig. 8.15a and b. The machine speed difference ω_B is mostly mono-modal, but the angle difference θ shows a distinct quasi-steady-state variation. Bandpass filtering is used to separate the oscillation and the quasi-steady-state components of δ, as shown in Fig. 8.16a and b. For the post-disturbance case, we get $x_e = 0.077$ pu from least-squares fitting, as in [21]. The equivalent machine inertia is estimated to be $H = 119$ pu. Figures 8.17a, b and 8.18 show the energy functions $\hat{V}_{\text{KE}}$, $\hat{V}_{\text{PE}}$, and $\hat{V}_E$, respectively. Note that oscillations are clearly visible in $\hat{V}_{\text{KE}}$ and $\hat{V}_{\text{PE}}$ and yet they literally disappear when $\hat{V}_{\text{KE}}$ and $\hat{V}_{\text{PE}}$ are added together to form $\hat{V}_E$. The oscillation is small-signal stable, although the damping is very low, and $\hat{V}_E$ eventually decays to a level commensurate with random perturbations on the system. If the system were negatively damped, $\hat{V}_E$ would grow. The quasi-steady-state angle δ_{qss} indicates that the sending end and receiving end of the transfer path remain synchronized, that is, transiently stable. A sudden increase in δ_{qss} indicates the loss of a portion of the transmission system or the loss of generation at the load bus, both of which would stress the transfer path. If the disturbance had caused a separation of the transfer path, δ_{qss} would grow as synchronism would be lost.

It is also worth noting that the amplitudes of oscillations in the interarea angular separation as well as frequency, following a disturbance, in two-area power systems, depend significantly on the strength of the interconnection as well as the inertia of the aggregated machines. We briefly illustrate this fact by comparing the maximum swing energy functions for two different transfer paths under two different sets of disturbances. We show that a comparison of energies of coherent machines forming interconnected transfer paths can be a good indication of the relative strengths of

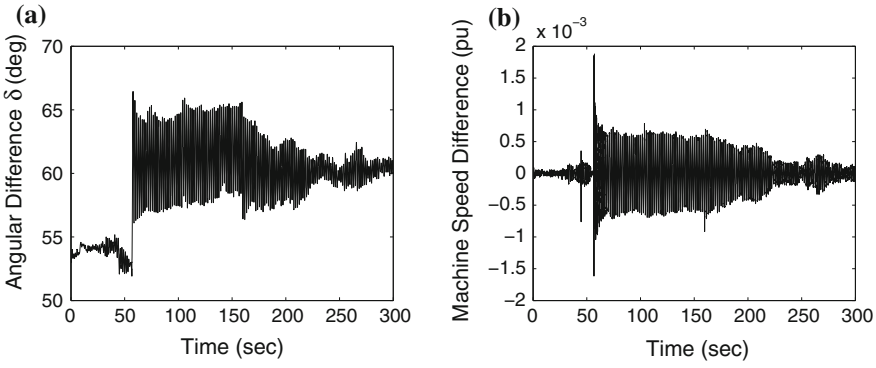

Fig. 8.15 Time variations of machine angle difference and machine speed difference in transfer path 1. **a** Machine angular difference δ (deg). **b** Machine frequency difference (pu)

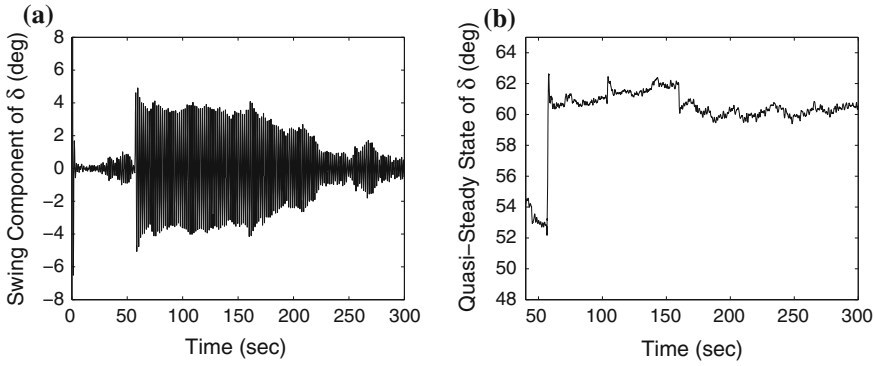

Fig. 8.16 Swing component and quasi-steady-state of machine angle difference in transfer path 1. **a** Swing component $\hat{\delta}$ on transfer path 1. **b** Quasi-steady-state δ_{qss} on transfer path 1

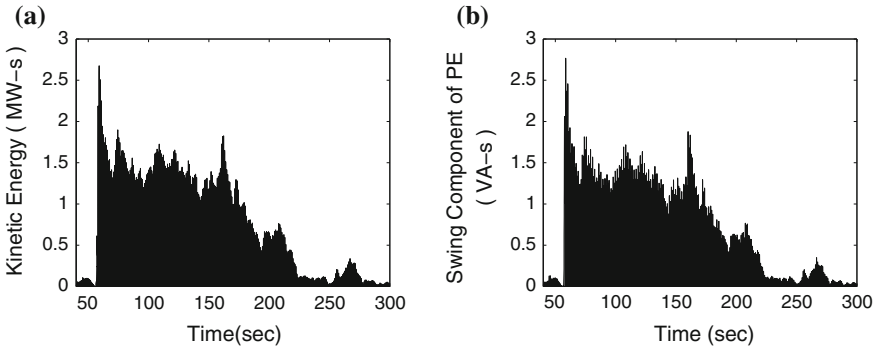

Fig. 8.17 Energy functions for transfer path 1. **a** Kinetic energy function for transfer path 1, **b** potential energy function for transfer path 1

disturbances on the transfer paths. Consider the interconnected power system with three aggregated machines as in Fig. 8.19. Generators 1 and 2 form a coherent group of machines (transfer path a) with power flowing from Generator 1 to 2, the inertia of Generator 1 being smaller than that of Generator 2. Generator 3 forms a coherent group with Generators 1 and 2 together (transfer path b), with the inertia of Generator 3 being significantly higher than that of Generators 1 and 2. The system has two interarea modes, namely a slower mode between G_3 and $(G_1,\ G_2)$, and a faster mode between G_1 and G_2 with much smaller amplitude. The line reactance, or equivalently connection strength, for transfer path a is weaker compared to that for path b. We consider two sets of disturbance events, namely Events 1 and 2, which caused perturbations in transfer paths a and b, respectively. Event 1 was actually caused by a control equipment failure with possible line tripping and, hence, did not produce any significant oscillations. Event 2, on the other hand, was an earthquake event leading to significant loss of load, due to which the oscillations were more

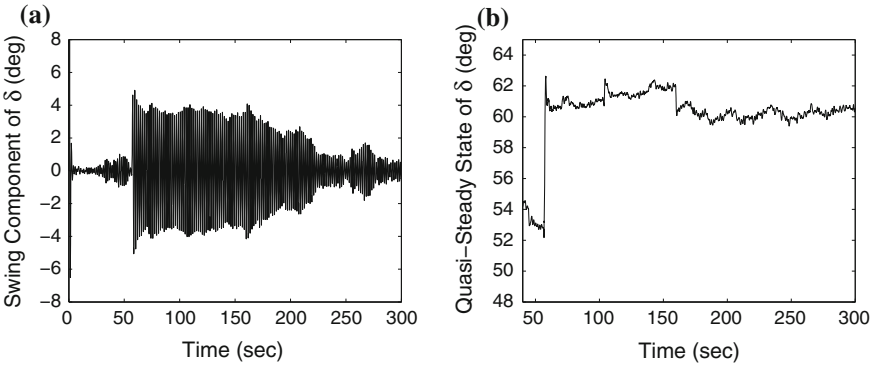

Fig. 8.18 Swing energy function for transfer path 1

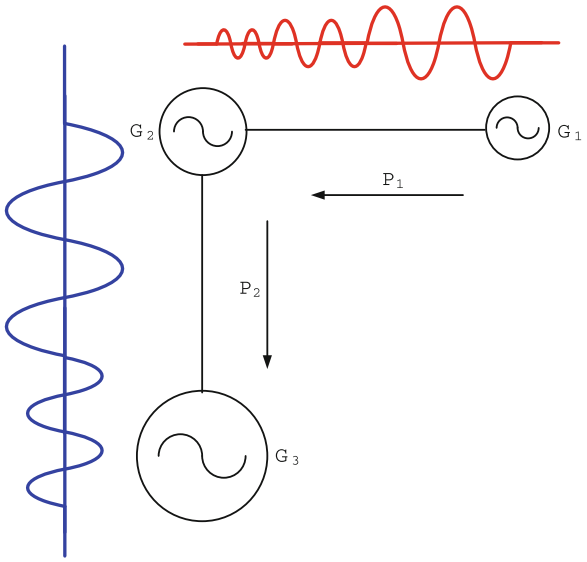

Fig. 8.19 Oscillations in two coherent areas for two events

pronounced. We next construct the swing energy functions for each transfer path for each event. Table 8.1 lists the maximum energy for each of these four cases. The numbers clearly indicate that the disturbance in transfer path *a* hardly caused any oscillations in transfer path *b* due to the high equivalent inertia of Generators 2 and 3, and the stronger connection strength between them. On the other hand, the disturbance in transfer path *b* resulted in a high energy value in transfer path *a* because of the lower machine inertia and connection strength of the latter.

Table 8.1 Swing energies of two paths for two disturbance events

Disturbance event	Maximum swing energy in path a	Maximum swing energy in path b
1	5 MW-s	0.33 MW-s
2	3.5 MW-s	17 MW-s

8.6 Equivalencing Using Noisy PMU Data

We end our discussion with a brief note on the situation where the aforesaid parameter estimation methods have to be carried out using PMU data corrupted with measurement noise. In that case, unique estimates of the model parameters are no longer available, and the problem has to be posed in terms of bounds on the estimation error. Such bounds, more commonly referred to as Cramer-Rao bounds (CRB), are widely used in the statistical signal processing literature [22]. By definition, CRB is a lower bound for the second-order moment of an unbiased parametric estimator. In this section we show an interesting fact: the CRB for estimating the *interarea* model parameters of a two-machine equivalent of the two-area radial power system of Sect. 8.2 is a function of the spatial variable a. In other words, the error in estimation depends on the location of the PMU on the transmission line. The problem, therefore, is to find the optimal location such that the estimation error is minimized.

Returning to the two-area power system model of Sect. 8.2, we linearize the model (8.6) about an initial equilibrium $(\delta_0,\ 0)$ where $0 < \delta_0 < 90^\circ$, and denote the perturbed state variables as $m = \text{col}(\Delta\delta,\ \Delta\omega)$ to obtain

$$\dot{m} = \underbrace{\begin{bmatrix} 0 & 1 \\ -\frac{E_1 E_2}{2Hx}\cos(\delta_0) & 0 \end{bmatrix}}_{A} m + \underbrace{\begin{bmatrix} 0 \\ 1 \end{bmatrix}}_{B} u \tag{8.84}$$

where u is a small disturbance input to the system. For any point P at reactance x away from Generator 2, the output matrix from (8.9) can be written as

$$C = \begin{bmatrix} \dfrac{-a(1-a)E_1 E_2 \sin(\delta_0)}{V_0} & 0 \end{bmatrix} \tag{8.85}$$

where $V_0 = \sqrt{E_2^2(1-a)^2 + E_1^2 a^2 + 2E_1 E_2 a(1-a)\cos(\delta_0)}$. After a few calculations, it can readily be shown that the discrete-time impulse response of the voltage at P is

$$V(k) = \psi(a)\,\xi(k, x_1, x_2, H_1, H_2) \tag{8.86}$$

where ξ for different values of k is listed in Table 8.2. We next stack the impulse response as

Table 8.2 Impulse response of undamped two-machine power system

k	$y(k)$
1	$\psi(a)\,K$
2	$\psi(a)\,K(1+2\cos(\sqrt{\gamma}T))$
3	$\psi(a)\,K(\cos(2\sqrt{\gamma}T))+2\cos(\sqrt{\gamma}T)(1+\cos(\sqrt{\gamma}T))$
$\vdots$	$\vdots$
n	$\psi(a)K\big(\cos((n-1)\sqrt{\gamma}T)+\left(\frac{1+\cos(\sqrt{\gamma}T)}{\sin(\sqrt{\gamma}T)}\right)$ $\sin((n-1)\sqrt{\gamma}T)\big)$

$$\mathscr{Y} = \big[\, y(1)\ y(2)\ \ldots\ y(k) \,\big]. \tag{8.87}$$

Assuming that unlimited time-series data are available, k can be any arbitrary positive integer. We partition the four unknown parameters x_1, x_2, H_1, and H_2 into sets $\mathbf{a} = \{x_1,\ x_2\},\ \mathbf{b} = \{H_1,\ H_2\}$ and define

$$\mathbf{H}(\mathbf{a},\ \mathbf{b}) = \partial\mathscr{Y}/\partial\mathbf{a}, \quad \mathbf{K}(\mathbf{a},\ \mathbf{b}) = \partial\mathscr{Y}/\partial\mathbf{b}. \tag{8.88}$$

Assuming that the actual measured PMU signal is

$$\tilde{y}(k) = y(k) + \tilde{n} \tag{8.89}$$

where $\tilde{n}$ is zero-mean Gaussian noise with variance σ^2, the Fisher Information Matrix for computing the error bounds is next formulated as

$$J(\mathbf{a}, \mathbf{b}) = \frac{1}{\sigma^2}\begin{bmatrix} \mathbf{H}\mathbf{H}^{\mathbf{T}} & \mathbf{H}\mathbf{K}^{\mathbf{T}} \\ \mathbf{K}\mathbf{H}^{\mathbf{T}} & \mathbf{K}\mathbf{K}^{\mathbf{T}} \end{bmatrix}. \tag{8.90}$$

Because CRB is the inverse of $J(\mathbf{a}, \mathbf{b})$, the tightest bound will be given by that value of a, say denoted as a^*, which maximizes the determinant of J. Moreover, as the PMU can only be placed on the transmission line, a^* must satisfy

$$a^* \in [a_1,\ a_2],\quad a_1 = \frac{x_2}{\bar{x}},\ a_2 = \frac{x_2 + x_e}{\bar{x}}. \tag{8.91}$$

Applying this procedure for the disturbance event of WECC transfer path 1 of Sect. 8.3, imposing a 10 dBW noise power on the actual measured data, the determinant of the FIM J plotted against $a \in [a_1,\ a_2]$ is shown in Fig. 8.20. From this figure, it follows that the best location P to place a PMU (or, equivalently consider a measurement from) is approximately at 40 % of the total length of the transmission line away from Bus 2, i.e., a reactance 0.0308 pu away from Bus 2, considering the output for estimation is the voltage magnitude at P. If any other variable such as the phase angle measured at P is used for estimating the parameters, then a different value of a^* will be obtained.

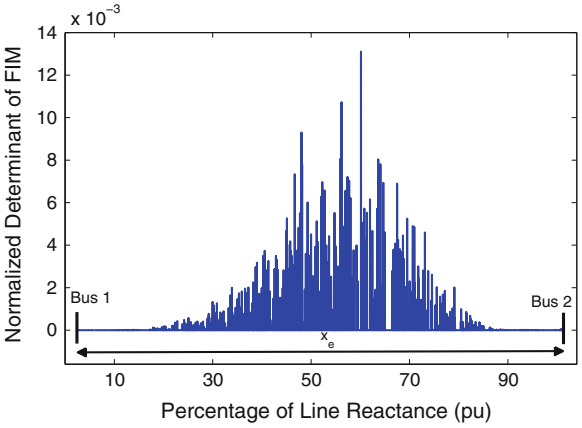

Fig. 8.20 Spatial variation of det(J)

8.7 Conclusions

In this chapter, we presented a collection of new results on model reduction of several classes of large-scale power systems using synchronized phasor data available only from a few selected points in the transmission network. The fundamental approach behind this model reduction is to formulate the reduction problem as an equivalent parameter estimation problem, which can be solved using the spatial variation of different phasor quantities from one end of the transfer path to another. The developed methods can be used to construct approximate interarea models of two representative transfer paths in the US west coast power system, each of which have been illustrated with real disturbance event data. Besides the natural benefits of model reduction, the advantage of such *dynamic equivalent* models lies in both wide-area monitoring and wide-area control. For example, these models can be directly used to construct transient energy functions operating across transfer paths, which in turn can be used as a performance metric to track the health of the interconnection following any large disturbance—in terms of damping, mode shape, rise time, settling time, etc., as shown in [21]. They will also be highly useful for efficient wide-area control designs at a global or *interarea* level. For instance, given the scale, size, and complexity of any realistic power system (e.g., WECC with roughly 2,000 generators, 11,000 transmission lines and 6,500 loads), designing PMU-based distributed controllers to shape the *interarea* responses starting from a full-order model would be highly daunting. We believe that an alternative approach of reducing such large systems into simpler chunks, and then redistributing their control efforts would give the problem a much more well-defined and less chaotic formulation. This work, however, should also be viewed as a point of departure for several future investigations. The variation of the IME model reactance as a function of power transfer levels and the correlation of fault clearing times between the IME model and the detailed model also need to be better understood.

References

1. A.G. Phadke, J.S. Thorp, M.G. Adamiak, New measurement techniques for tracking voltage phasors, local system frequency, and rate of change of frequency. IEEE Trans. Power Apparatus Syst. **102**, 1025–1038 (1983)
2. North American Synchrophasor Initiative (NASPI), www.naspi.org.
3. R.L. Cresap, J.F. Hauer, Emergence of a new swing mode in the western power system. IEEE Trans. Power Apparatus Syst. **PAS–100**(4), 2037–2045 (1981)
4. J. Ballance, B. Bhargava, G.D. Rodriguez, Use of synchronized phasor measurement system for enhancing AC-DC power system transmission reliability and capability, EIPP Meeting, Sep 2004
5. J.H. Chow, G. Peponides, P.V. Kokotović, B. Avramović, J.R. Winkelman, *Time-Scale Modeling of Dynamic Networks with Applications to Power Systems* (Springer, New York, 1982)
6. J.F. Hauer, C.J. Demeure, L.L. Scharf, Initial pesults in prony analysis of power system response signals. IEEE Trans. Power Syst. **5**(1), 80–89 (1990)
7. D.J. Trudnowski, J.W. Pierre, N. Zhou, J.F. Hauer, M. Parashar, Performance of three mode-meter block-processing algorithms for automated dynamic stability assessment. IEEE Trans. Power Syst. **23**(2), 680–690 (2008)
8. G. Ledwich, D. Geddy, P.O. Shea, Phasor Measurement Units for System Diagnosis and Load Identification in Australia, in *Proceedings of IEEE PES General Meeting*, Pittsburgh, PA, July 2008
9. D. Wilson, Oscillatory Mode Shape and Combined EMS/WAMS Data to Characterize and Locate Stability Issues, in *NASPI Meeting*, Charlotte, NC, Oct 2008
10. Q. Yang, T. Bi, J. Wu, WAMS Implementation in China and the Challenges for Bulk Power System Protection, in *Proceedings of IEEE PES General Meeting*, Tampa, FL, July 2007
11. J. Rasmussen, A.H. Nielsen, Phasor Measurement of Wind Power Plant Operation in Eastern Denmark, in *European Offshore Wind Conference & Exibition*, Berlin, Germany, 2007
12. A.J. Germond, R. Podmore, Dynamic aggregation of generating unit models. IEEE Trans. Power Apparatus Syst. **PAS–97**(4), 1060–1069 (1978). (July/Aug)
13. R.W. de Mello, R. Podmore, K.N. Stanton, Coherency-Based Dynamic Equivalents: Applications in Transient Stability Studies, in *Proceedings of PICA Conference*, New Orleans, LA, June 1975, pp. 23–31
14. J.M. Undrill, A.E. Turner, Construction of power system electromechanical equivalents by modal analysis. IEEE Trans. Power Apparatus Syst. **PAS–90**, 2049–2059 (1971)
15. J. Zaborszky, K.W. Whang, G. Huang, L.J. Chiang, S.Y. Lin, A clustered dynamic model for a class of linear autonomous system using simple enumerative sorting. IEEE Trans. Circuits Syst. **CAS–29**(11), 747–758 (1982). (Special Issue)
16. R. Nath, S.S. Lamba, K.S.P. Rao, Coherency based system decomposition into study and external areas using weak coupling. IEEE Trans. Power Apparatus Syst. **PAS–104**, 1443–1449 (1985)
17. W.W. Price, G.E. Boukarim, J.H. Chow, R. Galarza, A.W. Hargrave, B.J. Hurysz, R. Tapia, Improved Dynamic Equivalencing Software, Final Report, EPRI Project RP2447-02, 1995
18. A.R. Bergen, V. Vittal, *Power System Analysis*, 2nd edn. (Prentice Hall, NJ, 1999)
19. J.J. Sanchez-Gasca, J.H. Chow, Performance comparison of three identification methods for the analysis of electromechanical oscillations. IEEE Trans. Power Syst. **14**(3), 995–1002 (1999)
20. A. Chakrabortty, *Estimation, Analysis and Control Methods for Large-scale Electric Power Systems using Synchronized Phasor Measurements*. Ph.D Dissertation, Rensselaer Polytechnic Institute, Troy, NY, 2008
21. J.H. Chow, A. Chakrabortty, M. Arcak, B. Bhargava, A. Salazar, Synchronized phasor data based energy function analysis of dominant power transfer paths in large power systems. IEEE Trans. Power Syst. **22**(2), 727–734 (2007)
22. T. McWhorter, L.L. Scharf, Cramer-Rao bounds for deterministic modal analysis. IEEE Trans. Signal Process. **41**(5), 1847–1865 (1993)

23. A. Chakrabortty, J.H. Chow, A. Salazar, A Measurement-based Framework for Dynamic Equivalencing of Large Power Systems using WAMS, in *Proceedings of IEEE PES Conference on Innovative Smart Grid Technologies*, Jan 2010
24. N.L. Biggs, E.K. Lloyd, R.J. Wilson, *Graph Theory* (Oxford University Press, Oxford, 1976)